Deciphering deep-sea chemosynthetic symbiosis by single-nucleus RNA-sequencing

Hao Wang[1,2,3,4#], Kai He[5#], Huan Zhang[1#], Quanyong Zhang[6#], Lei Cao[1], Jing Li[1,7], Zhaoshan Zhong[1], Hao Chen[1], Li Zhou[1], Chao Lian[1], Minxiao Wang[1], Kai Chen[6], Pei-Yuan Qian[3,4*], and Chaolun Li[1,7,8*]

[1]Center of Deep-Sea Research, Institute of Oceanology, Chinese Academy of Sciences, Qingdao, China

[2]Laboratory for Marine Biology and Biotechnology, Qingdao National Laboratory for Marine Science and Technology, Qingdao, China

[3]Southern Marine Science and Engineering Guangdong Laboratory (Guangzhou), Nansha, Guangzhou, China

[4]Department of Ocean Science, Hong Kong University of Science and Technology, Hong Kong S.A.R, China.

[5]Key Laboratory of Conservation and Application in Biodiversity of South China, School of Life Sciences, Guangzhou University, Guangzhou, Guangdong 510006, China

[6]State Key Laboratory of Primate Biomedical Research, Institute of Primate Translational Medicine, Kunming University of Science and Technology, Kunming, China

[7]South China Sea Institute of Oceanology, Chinese Academy of Sciences, Guangzhou, China

[8]University of Chinese Academy of Sciences, Beijing, China

Correspondence authors: Prof. Pei-yuan Qian and Prof. Chaolun Li

Email addresses: boqianpy@ust.hk and lcl@qdio.ac.cn

#These authors contributed equally to this work

The authors declare no conflict of interest.

Abstract:

Bathymodioline mussels dominate deep-sea methane seep and hydrothermal vent habitats and obtain nutrients and energy primarily through chemosynthetic endosymbiotic bacteria in the bacteriocytes of their gill. However, the molecular mechanisms that orchestrate mussel host-symbiont interactions remain unclear. Here, we constructed a comprehensive cell atlas of the gill in the mussel *Gigantidas platifrons* from the South China Sea methane seeps (1100m depth) using single-nucleus RNA sequencing (snRNA-seq) and whole-mount *in situ* hybridisation. We identified 13 types of cells, including three previously unknown ones, and uncovered unknown tissue heterogeneity. Every cell type has a designated function in supporting the gill's structure and function, creating an optimal environment for chemosynthesis, and effectively acquiring nutrients from the endosymbiotic bacteria. Analysis of snRNA-seq of *in situ* transplanted mussels clearly showed the shifts in cell state in response to environmental oscillations. Our findings provide insight into principles of host-symbiont interaction and the bivalves' environmental adaption mechanisms.

15 **Introduction:**

16 Mutualistic interactions between multicellular animals and their microbiota play a funda-
17 mental role in animals' adaptation, ecology, and evolution [1,2]. By associating with symbionts,
18 host animals benefit from the metabolic capabilities of their symbionts and gain fitness advan-
19 tages that allow them to thrive in habitats they could not live in on their own[1,3]. Prime exam-
20 ples of such symbioses are bathymodioline mussels and gammaproteobacteria endosymbionts[4].
21 The bathymodioline mussels occur worldwide at deep-sea chemosynthetic ecosystems, such as
22 cold-seeps, hydrothermal vents, and whale falls[4]. The host mussel acquired sulfur-oxidising
23 (SOX) and/or methane-oxidising (MOX) symbiont through horizontal transmission at their early
24 life stage[3]. Their symbionts, which are hosted in a specialised gill epithelial cell, namely, the
25 bacteriocytes[5,6], utilise the chemical energy from the reduced chemical compounds such as CH_4
26 and H_2S released from cold seeps or hydrothermal vents to fix carbon and turn into carbon
27 source for the host mussel[7,8]. The ecological success of the bathymodioline symbioses is appar-
28 ent: the bathymodiolin mussels are often among the most dominant species in the deep-sea
29 chemosynthetic ecosystems[9,10]. Thus, it is critical to know how the bathymodioline mussels in-
30 teract with the symbionts and maintain the stability and efficiency of the symbiosis.

31 The gill structure of bathymodiolin mussels has undergone remarkable adaptations at the
32 molecular, cellular, and tissue levels to support their deep-sea chemosynthetic lifestyle[11,12].
33 Compared to shallow water mussels[13], the gill filaments of bathymodiolin mussels have
34 enlarged surfaces allowing them to hold more symbionts per filament (Supplementary Fig. S1).
35 This adaption requires not only novel cellular and molecular mechanisms to maintain and sup-
36 port the enlarged gill filament structure, but also a strong ciliary ventilation system to pump
37 vent/seep fluid to fuel the symbiotic bacteria. Previous studies based on whole-genome se-
38 quencing and bulk RNA-seq projects have shown that genes in the categories of nutrient trans-
39 porters, lysosomal proteins, and immune receptors are either expanded in the host mussel's
40 genome or up-regulated in the gill[12, 14-17], suggesting that these genes involved in host-symbiont
41 interaction. Though providing deep molecular insights, these studies mainly used homogenised
42 tissues that average genes' expression levels amongst different cell types and eliminate cell and
43 gene spatial distribution information[18-21]. In addition, the broad expression and function of po-

44 tentially 'symbiosis-related' proteins also greatly limited data interpretation. Therefore, a sys-
45 temic atlas of gill cell types and the descriptions of cell-type-specific gene expressional profiles
46 are warranted to a better understanding of the host-symbiont interaction and environmental
47 adaptation mechanisms of the bathymodioline symbiosis.

48 In recent years, single cell/nucleus RNA-sequencing (sc/sn RNA-seq) technologies have be-
49 come one of the preferred methods for investigating the composition of complex tissue at the
50 transcriptional level[22]. snRNA-seq has several advantages, such as compatibility with frozen
51 samples, elimination of dissociation-induced transcriptional stress responses, and reduced dis-
52 sociation bias[23]. These advantages are significant for deep-sea and other ecological studies be-
53 cause cell and molecular biology facilities are not available in the field. To examine the cellular
54 and molecular mechanisms of the environmental adaptations and host-symbiont interactions in
55 bathymodioline mussels, we conducted a single nucleus RNA-sequencing-based transcriptomic
56 study. We analysed the gill symbiosis in the dominate deep-sea mussels inhabiting the F-site
57 cold-seep *Gigantidas platifrons*[24], which hosts a single a MOX endosymbiont population that
58 consist of only one 16S rRNA phylotype. Our work provides a proof-of-principle for environ-
59 mental adaptation mechanisms study in non-traditional but ecologically important organisms
60 with single-nucleus RNA-sequencing technologies.

Results and discussion

1. *G. platifrons* deep-sea *in situ* transplant experiment and single-cell transcriptomic sequencing:

We conducted a *G. platifrons* deep-sea *in situ* transplant experiment at the "F-Site" Cold-seep (~1117 m depth) and retrieved three groups of samples (Fig. 1A), as follows: the 'Fanmao' (meaning prosperous) group, which comprised the mussels collected from methane-rich (~40 µM) site of the cold-seep, where the animals thrived; the 'starvation' group, which comprised the mussels collected from the methane-rich site and then moved to a methane-limited (~0.054 µM) starvation site for 14 days before retrieval; and the 'reconstitution' group, which comprised the methane-rich site mussels moved to the 'Starvation' site for 11 days and then moved back to the methane-rich site for another 3 days.

We next performed single nucleus RNA-sequencing (snRNA-seq) of the gill posterior tip of the three groups of samples using the microwell-based BD Rhapsody platform™ Single-Cell Analysis System (Fig. 1A). After quality control, we obtained 9717 (Fanmao), 21614 (Starvation), and 28928 (Reconstitution) high-quality single nuclei transcriptomic data.

2. Cell atlas of *G. platifrons gill*

To unravel the intricate cellular composition, we utilised a reciprocal PCA (RPCA) strategy to project cells in the three samples onto the same space based on conserved expressed genes among them[25]. This strategy maximises the number of cells per cluster regardless of the organism's state and therefore maximises genes per cluster[26].

Through the implementation of Seurat, we revealed 14 cell clusters, each was associated with a set of marker genes (Figs. 1B- D) [27,28]. Given the limited availability of canonical marker genes for *G. platifrons* and molluscs in general, we undertook a meticulous approach to characterize each cell cluster. This involved: 1) examining the cluster marker genes' functions, 2) identifying the expression pattern of cluster marker gene using whole-mount *in situ* hybridisation (WISH) and/or double-fluorescent *in situ* hybridisation (FISH) analyses, and 3) conducting scanning electron microscopy (SEM) and transmission electron microscopy (TEM) analyses. We successfully identified and characterized 13 of the 14 cell clusters, which could be categorized into

90 four major groups, including 1) the supportive cells, 2) the ciliary cells, 3) the proliferation cells,
91 and 4) the bacteriocytes. One cell cluster remained ambiguous. To assess the robustness of
92 each cell cluster, we employed a bootstrap sampling and clustering algorithm examining the
93 similarity among clusters and obtained strong support for all clusters through a combined
94 analysis of the three samples (Supplementary Fig. S2A). Furthermore, when examining each
95 sample individually, we found that the majority of clusters demonstrated robust support, with
96 the exception of the three ciliary cell clusters, which showed overlaps of assignment probabili-
97 ties among them (Supplementary Fig. S2 B-D). These three cell types are derived from a same
98 precursor, and exhibited relatively lower numbers of nuclei, resulting in a reduced availability of
99 genes per cell type, which is particularly true for the food grove ciliary cell (Supplementary Ta-
100 ble S1). By integrating the spatial and functional annotations of these cell clusters, we gained
101 insight into their collective efforts in supporting the symbiotic relationship and maintaining the
102 high-efficiency chemosynthetic system within the gill tissue.
103 **Supportive cells:** We have identified four supportive cell types, namely, inter lamina cells
104 basal membrane cells (BMC)1, BMC2, and mucus cells (Figs 2A, B and C).
105 The inter lamina cells, marked by high expression of fibrillar-forming collagens, were the
106 cells located between the two layers of basal membranes (Fig 2D and E). These cells were pre-
107 viously identified as amoeboid cells[13], and their function has not been explored. The inter lam-
108 ina cells were densely distributed around the food groove and at the rim of the gill filament.
109 While on the middle part of the gill filament, the inter lamina cells distributed in parallel rows. It
110 might help to connect the two sheets of basal membranes and maintain the spatial integrity of
111 the gill filament. In addition, we observed the enrichment of ribosomal proteins involved in
112 protein synthesis (Supplementary Table S2), indicating a high metabolic rate[29] of inter lamina
113 cells. This implies that the inter lamina cells may process the nutrients acquired from the sym-
114 biont.
115 We have also identified two types of BMC populations which have not been recognised be-
116 fore. The BMC1 (Fig. 2F and G) expressed genes encoding extracellular matrix and adhesive pro-
117 teins (Fig. 2B and Supplementary Table S2), such as SCO-spondin (Bpl_scaf_27638-4.18),
118 Zonadhesin (Bpl_scaf_1371-2.4), Cartilage matrix proteins (Bpl_scaf_16371-0.14 and

119 Bpl_scaf_3387-5.47), and Collagen alpha-1(XXI) chain protein (Bpl_scaf_51350-0.19). BMC2 (Fig.
120 2H and I) was distinctive from BMC1 in the context of expression (Fig 2A) and marker genes (Fig
121 2B). Genes encoding hemicentins (Bpl_scaf_38731-0.50 and Bpl_scaf_7293-0.14), which are
122 known to stabilise the cells' contact with the basal membrane[30], were highly expressed in BMC2.
123 Thus, these two cell types are likely to help building the basal lamina, and stabilising the epithe-
124 lial-derived cells, such as bacteriocytes and intercalary cells, on the surface of the basal mem-
125 brane.

126 Mucus cells are specialised secretory cells with intracellular mucus vacuoles[13]. In shallow-
127 water filter-feeding bivalves, mucus cells secret mucus, which cooperates with the ciliary venti-
128 lation system to capture, process, and transport food particles to their mouths, known as filter
129 feeding mechanism[31-34]. Deep-sea mussels may not necessarily retain this function since they
130 do not normally acquire food resources such as phytoplankton and planktonic bacteria but ob-
131 tain most of nutrient through their chemosynthetic symbiont. Thus, it was hypothesised that
132 mucus cells are involved in other biological functions such as immune responses to pathogens[18].
133 Herein, genes encoding proteins with microbe-binding functionalities were enriched in mucus
134 cells (Fig. 2B and Supplementary Table S2), such as C-type lectins (Bpl_scaf_58694-0.22 and
135 Bpl_scaf_38133-0.8), C1q domain-containing protein (Bpl_scaf_55216-2.11), and Fibrinogen C
136 domain-containing protein (Bpl_scaf_18519-2.15)[35,36]. The expression of similar immune genes
137 was upregulated in a shallow water mussel *Mytilus galloprovincialis* when challenged by a
138 pathogenic bacteria[37]. Our WISH and double-FISH analyses showed that mucus cells were em-
139 bedded within the outer rim cilia and scattered on the gill lamella alongside the bacteriocytes
140 (Figs. 2J and 2K). These data collectively suggest that mucus cells may help mussel maintain the
141 immune homeostasis of gill. Interestingly, WISH and double-FISH analyses showed that mucus
142 cells were also distributed alongside the gill lamella's food groove and the inner edge, where
143 the density of bacteriocytes is low (Fig. 2J). Because the food groove is the main entry of food
144 practical to the labial palps and mouth[38], this distribution pattern implies that mucus cells may
145 be also involved in capturing planktonic bacteria and sending them to the mouth.

146 **Ciliary and smooth muscle cells:** A remarkable feature of bathymodioline mussel's gill is its
147 ciliary ventilation system, which constantly agitates the water and provides the symbiont with

148 the necessary gas[39]. We identified four types of ciliary cells (Figs. 3A and 3B): apical ridge ciliary
149 cells (ARCCs), food groove ciliary cells (FGCCs), lateral ciliary cells (LCCs), and intercalary cells
150 (ICs), as well as a newly identified type of smooth muscle cells. All ciliary cells were marked by
151 canonical cilium genes, such as genes encoding flagellar proteins, ciliary motor kinesin proteins,
152 ciliary dynein proteins, and ciliary microtubules and were clearly distinguishable by specifically
153 expressed genes (Supplementary Table S3 and Supplementary Fig. S3). ARCCs were character-
154 ized by expression of Tubulin alpha-1A chain Bpl_3489-0.37 (Fig. 3C) and Bpl_scaf_20631-1.16,
155 which encodes homeobox Dlx6a-like protein (Fig. 3D) which is a marker of the apical ectoder-
156 mal ridge[40]. FGCCs, which could be ladled by expression of marker gene Bpl_scaf_5544-0.0 (Fig.
157 3E), expressed genes encoding primary cilia development regulator Tubby-related protein 3[41]
158 (Bpl_scaf_24834-2.3) and primary ciliary cell structural protein TOG array regulator of axonemal
159 microtubules protein 1[42,43] (Bpl_scaf_55620-1.3), suggesting the FGCCs are the sensory ciliary
160 cells that gather information from the surrounding environment. Both ARCCs and FGCCs were
161 located around the ventral tip of the gill filament (Fig. 3F). LCCs were distributed as two parallel
162 rows along the gill lamella's outer rim and ciliary disks' outer rim (Figs. 3G and 3H) and had
163 highly expressed genes involved in cilium structure, cilium movement and ATP synthases (Fig.
164 3B and Supplementary Table S3), indicating that LCCs may have a strong ability to beat their
165 cilia. Interestingly, we identified a group of previously unreported smooth muscle cells (SMCs)
166 co-localised with the LCCs as showed by WISH (Fig. 3I and Supplementary Fig. S4). SMCs
167 strongly expressed several Low-density lipoprotein receptors (LDL receptor) and LDLR-
168 associated proteins[44] (Fig. 3B). In addition, these cells also expressed the angiotensin-
169 converting enzyme-like protein[45] (Bpl_scaf-29477-5.10) and the 'molecular spring' titin-like pro-
170 tein[46] (Bpl_scaf_56354-7.8) (Supplementary Table S3). The expression of these genes could be
171 commonly found in human vascular smooth muscle cells[47-49]. Collectively, we suspect that SMCs
172 are involved in lateral cilium movement and the gill slice contraction.
173 ICs are the specialised ciliary cells surrounding the bacteriocytes (Figs. 3B and 3J). WISH
174 analysis showed that the expressions of IC markers had apparent spatial variations (Fig. 3J). The
175 expression of ICs marker rootletin[50-52] (Bpl_scarf_22362-6.9) was considerably higher in the ICs
176 close to the frontal edge of the gill filament, and the expression gradually decreased along with

177 the direction of inter lamina water flow (Fig. 3K and Supplementary Fig. S5), implying that ICs
178 ventilate the water flow and the mucus through the gill filaments. Furthermore, compared with
179 the other three types of ciliary cells, the ICs expressed several genes encoding transcription fac-
180 tors involved in determining cell fate (Fig. 3B and Supplementary Table S3), such as transcrip-
181 tion factors Sox 8 (Bpl_scarf_40595-5.30) and Wnt pathway cell polarity regulator secreted friz-
182 zled-related protein 5 (Bpl_scaf_57424-6.1)[53], suggesting that the ICs might also play regulatory
183 roles[54-56].

184 **Proliferation cells**: It has long been known that the bathymodioline mussel gill has three
185 types of proliferation cells that are conserved throughout all filibranchia bivalves: the budding
186 zone at the posterior end of the gill where new gill filaments are continuously formed, and the
187 dorsal and ventral ends of each gill filaments[57,58]. These "cambial-zone"-like cell populations
188 could continuously proliferate throughout the whole life span of the mussel[58]. Our snRNA-seq
189 data recognised three types of proliferation cells, which is consistent with previous findings (Fig.
190 4A, Fig. 4B and Supplementary Table S4). The gill posterior end budding zone cells (PEBZCs) are
191 located on the first few freshly proliferated filaments of the posterior tip of gill (Figs. 4C and 4D).
192 The PBEZCs marker (Bpl_scaf_61993-0.4) gradually disappeared at around the 11th -12th row
193 of the gill filament (Fig. 4D), suggesting the maturation of the gill filaments, which is similar to
194 the developmental pattern reported in another deep-sea mussel *Bathymodiolus azoricus* [59]. The
195 dorsal end proliferation cells (DEPCs), which expressed the hallmarks genes of muscular tissue
196 (Fig. 4B), as well as cell proliferation and differentiation regulators, were the proliferation cells
197 in connective tissue at the dorsal end of the gill slice (Fig. 4A, 4E). The ventral end proliferation
198 cells (VEPCs) were two symmetrical triangle-shaped cell clusters of small symbiont-free cells
199 (Fig. 4F). In VEPCs, genes encoding ribosomal proteins, chromatin proteins, RNA and DNA bind-
200 ing proteins, and cell proliferation markers were all up-regulated (Fig. 4B and Supplementary
201 Table S4), indicating that VEPCs are meristem-like cells[59,60].

202 It has been hypothesised that new proliferation cells will be colonised by symbionts, serving
203 as the vital mechanism of bacteriocyte recruitment[59]. We then determined which proliferation
204 cell type gives rise to the mature cells, especially the bacteriocytes, which has little available
205 information regarding their precursor and transmission mode in bathymodioline mussels [59,61].

206 Slingshot trajectory analysis suggested that the PEBZCs might be the origin of all gill epithelial
207 cells, including the other two proliferation cells (VEPC and DEPC) and bacteriocytes (Supple-
208 mentary Fig. S6). The sole exception was BMC2, which may be derived from VEPC rather than
209 PEBZC. This result is consistent with previous studies which suggested new gill filaments of the
210 filibranch mussels are formed in the gill's posterior budding zones[59]. The colonisation by the
211 symbiont might play a crucial role in determining the fate of the bacteriocytes. Noticeably, in *G.*
212 *platifrons*, only the pillar-shaped first row of gill filament, comprised of small meristem-like cells,
213 was symbiont-free (Figs. 4D and D'), whereas all the other gill filaments were colonised by sym-
214 bionts. This pattern of symbiosis establishment is different from that of *B. azoricus*, in which
215 PEBZCs are symbiont free and are gradually colonised by symbionts released from the bacterio-
216 cytes on the adjacent mature gill filaments after maturation[59]. On mature gill filaments, the
217 DEPCs and VEPCs are seemingly the sources of new cells that sustain the growth of the gill fila-
218 ment from both dorsal and ventral directions, respectively[57]. Interestingly, comparable active
219 ventral and dorsal end proliferation zones have also been identified in the symbiotic mussel *B.*
220 *azoricus*, whereas they are absent in the shallow-water mussel *Mytilus edulis*[62]. This contrast
221 further suggests the potential involvement of DEPCs and VEPCs in the establishment of symbio-
222 sis.
223
224 **3. Bacteriocytes and host-symbiont interaction:**
225 We conducted the whole-mount FISH using a bacterial 16S rRNA probe for symbiont to de-
226 termine the spatial distribution of bacteriocytes, and their positions relative to the other cell
227 types on the gill filament (Figs. 5A, B). Bacteriocytes covered the majority of the surface of the
228 gill filament, except the ventral tip, the ciliary disk, and the frontal edge (lateral ciliary). The
229 bacteriocytes were surrounded by intercalary cells with microvilli and cilia on the surface (Fig.
230 5C).
231
232 The gene expression profile of bacteriocytes aligned well with the morphological analysis,
233 which suggested that the bacteriocytes have structural, metabolic, and regulatory adaptions to
234 cope with the symbiont (Figs. 5D, 5F and 5I). It has been hypothesised that the bacteriocytes

235 extract nutrients from the symbiont through two pathways: lysing the symbiont through the
236 lysosome (the 'farming' pathway) or directly utilising the nutrient produced by the symbiont
237 (the 'milking' pathway)[63,64]. Our TEM observations clearly detected intracellular vacuole and
238 lysosome system of the bacteriocyte that harbour, transport, and digest the symbionts (Fig. 5D),
239 which is consistent with previous studies[18,65]. The snRNA data showed bacteriocytes expressed
240 cellular membrane synthesis enzyme (phosphoethanolamine N-methyltransferase,
241 Bpl_scaf_15282-3.10) and a series of lysosomal proteins such as lysosomal proteases (cathep-
242 sins; Bpl_scaf_61711-5.12, Bpl_scaf_46838-6.40 and Bpl_scaf_59648-4.5; lysosomal alpha-
243 glucosidase-like), protease regulators 56 (TMPRSS15 proteins; Bpl_scaf_52188-1.15 and
244 Bpl_scaf_15410-0.9), and lysosomal traffic regulator proteins (rabenosyn-5, Bpl_scaf_54816-0.3
245 and Bpl_scaf_52809-1.6, lysosomal-trafficking regulator-like isoform X1). Among the proteases,
246 cathepsins were thought to be evolutionary conserved molecular tools that host utilized to con-
247 trol the residence of their symbiont microbes[66]. They were also highly expressed in symbiotic
248 tissue of other deep-sea chemosynthetic animals, such as vesicomyid clams and vestimen-
249 tiferan tubeworms[67-69]. Bacteriocytes also expressed genes encoding cellular vesicle transports
250 (kinesins, Bpl_scaf_14819-0.11, Bpl_scaf_54265-1.13, and Bpl_scaf_4784-1.40)[53], potential
251 amino acid transporter[57] (Bpl_scaf_36159-5.5), and genes involved in intracellular vesicle trans-
252 port, such as the FYVE and coiled-coil domain-containing protein 1[58] (Bpl_scaf_33726-5.7). In
253 addition to form and mobilise early endosomes, the protein products of these genes could
254 transport symbiont-secreted nutrient vesicles to the host (Fig. 5F and Supplementary Table S5),
255 supporting the “milking” pathway.
256 The symbiont of *G. platifrons* belongs to type I methanotrophy, of which the core metabolic
257 function is linked with the development of intracytoplasmic membranes leading to a high
258 lipid/biomass content[70,71]. Recent lipid biomarker analyses showed that the gill of *G. platifrons*
259 contains a high amount of bacterial lipids, which are directly utilised by the host to synthesise
260 most of its lipid contents[67]. Downstream of the bacteriocyte’s metabolic cascade, genes encod-
261 ing proteins that may be involved in fatty acid/lipid metabolism, such as perilipin2
262 (Bpl_scaf_27158-3.8), which is the critical protein to form intracellular lipid droplets[72], and a
263 variety of fatty acid metabolism enzymes (acetyl carboxylase 2, Bpl_scaf_55250-5.11[73]; fatty

264 acid desaturase 1-like isoform X1, Bpl_scaf_35916-0.6[74,75]; long-chain fatty acid-ligase ACSBG2-
265 like isoform X1, Bpl_scaf_28862-1.5 [76,77]), were up-regulated, suggesting that the fatty acid
266 could be a major form of nutrients passing from the symbiont to the host mussel.
267 Additionally, bacteriocytes expressed several solute carriers, including sodium/ascorbate co-
268 transporter (Fig. 5I, solute carrier family 23 members 1-like, Bpl_scaf_32311-1.19), so-
269 dium/potassium/calcium exchanger (sodium potassium calcium exchanger 3-like,
270 Bpl_scaf_14503-1.28), sodium/chloride ion cotransporter (solute carrier family 12 member 3-
271 like isoform X1, Bpl_scaf_44604-3.7), ferrous iron transporter (solute carrier family 40 member
272 1-like, Bpl_scaf_63447-0.12) and zinc transporter (zinc transporter ZIP14-like, Bpl_scaf_44428-
273 5.3). The solute carriers are a large family of ATP-dependent transporters that shuttle a variety
274 of small molecules across the cellular membrane[78]. In several model symbiotic systems, solute
275 carriers play a vital role in host-symbiont interaction by either providing the symbiont with sub-
276 strates[79,80] or transporting symbiont-produced nutrients to the host [81-83]. Previous studies dem-
277 onstrated that solute carrier genes were expanded in deep-sea chemosynthetic animals' ge-
278 nome[84] and highly expressed in symbiotic organs[85] including bathymodioline mussel's gill[12]. In
279 bathymodioline mussels, previous bulk RNA-seq studies detected up-regulated expression of a
280 large variety of solute carriers in the gill, which is consistent with the present study, suggesting
281 that solute carriers may play crucial roles in shuttling nutrients in and out of bacteriocytes and
282 in maintaining the suitable intracellular micro-environment (such as the SLC23A1 and SLC39A14)
283 for the symbiont[86,87].
284
285 **4. Cell-type-specific response to environmental stresses:**
286 To examine cell-type-specific acclimatisation to environmental changes the expression pro-
287 files of differentially expressed genes (DEGs) were compared between the three states (Fanmao,
288 starved and reconstituted animals) of samples collected in our *in situ* transplantation experi-
289 ment (full lists of DEGs are shown in Supplementary Table S6-S18). Notably, for each state three
290 mussels were processed but pooled for nuclei extraction before snRNA sequencing (see
291 Method for detail). We tested our hypothesis here that at the starvation site, a relatively low
292 concentration of methane shall upset symbiont metabolism and thus substantially affect sym-

293 biont-hosting bacteriocytes by assessing the transcriptional changes per cell type. We calcu-
294 lated the distances between the three sets of samples on the UMAP plot (Fig. 6A) estimating
295 the centroid coordinates per sample per cell type, and calculating the Euclid distance between
296 the centroid coordinates of each pair of states per cell type (Supplementary Table S19). The im-
297 pact of starvation was variable across cell types, as reflected by the cross-state distances (Fig.
298 6B, green bar). Starvation resulted in the most significant transcriptional changes in bacterio-
299 cytes reflected by a large Fanmao-vs-starvation distance (2.3), followed by VEPC and inter lam-
300 ina cells (2.1 and 1.4, respectively). On the other hand, starvation had little impact on the tran-
301 scriptions of ciliary cells and most supportive cells such as the food grove ciliary cell, BMC2, and
302 mucus cells (distances <0.5). Fig 6B also shows that after reconstitution (moving the mussels
303 back to the methane-rich site Fanmao for 3 days), the expressional profile of bacteriocytes rap-
304 idly changed back, reflected by a large starvation-vs-reconstitution distance and much smaller
305 Fanmao-vs-reconstitution distance (2.3 vs. 0.8; Suppl. Tab. S19). This result coincided with and
306 was supported by our pseudo-time analysis for bacteriocytes (Fig. 6C), showing that bacterio-
307 cytes in the reconstitution are in intermediate and transitional states between Fanmao and
308 starvation.
309 For the bacteriocytes population, we conducted cell trajectory pseudo-timing and detailed
310 DEG analysis to interpret the mechanism of host-symbiont interactions. It is important to
311 acknowledge that our sampling strategy might have limitations, as more closely spaced time
312 points could enhance the confidence of trajectory reconstruction. The branched heatmap
313 showed both up- and down-regulated genes during starvation and reconstitution compared
314 with the Fanmao state (Fig. 6D and supplementary Fig. S7). The Kyoto Encyclopedia of Genes
315 and Genomes (KEGG) pathway enrichment analysis of the bacteriocytes' DEGs provides an
316 overall view of the pathways enriched in each environmental state (Supplementary Fig. S8 A-C).
317 The genes encoding ribosomal proteins are highly expressed in the bacteriocytes under the
318 methane-rich 'Fanmao' state (Supplementary Fig. S8A), suggesting an active protein synthesis
319 and cellular metabolism [88]. Moreover, organic ion transporters (A BCB P-glycol,
320 Bpl_scaf_18613-16.10; canalicular multispecific organic anion transporter 2, Bpl_scaf_52110-
321 4.43; sodium- and chloride-dependent glycine transporter 1-like, Bpl_scaf_13642-5.8), which

322 may be involved in transporting symbiont-produced nutrients, are also highly expressed (Sup-
323 plementary Fig. S9).
324 In starved *G. platifrons*, negative regulators of cell proliferation, such as autocrine prolifera-
325 tion repressors and receptor-type tyrosine phosphatase beta, were up-regulated in bacterio-
326 cytes, suggesting repression of cell growth. We also observed the enrichment of genes in the
327 apoptosis pathway (Supplementary Fig. S8B), which is attributed to the upregulation of cas-
328 pases (Bpl_scaf_25165-3.8 and Bpl_scaf_24225-0.12) and cathepsins (Bpl_scaf_64706-0.16,
329 Bpl_scaf_61711-5.12) which can trigger caspases-dependent cell death, suggesting cellular
330 stress condition. Correspondingly, a gene encoding baculoviral IAP repeat-containing protein
331 (Bpl_scaf_6172-0.3), which can bind caspase and inhibit apoptosis, was up-regulated in bacte-
332 riocytes (Fig. 6E). In *Drosophila*, the baculoviral IAP proteins are important in animal's response
333 to cellular stress and promote cell survival[89,90]. Similarly, the gene encoding MAP3K14
334 (Bpl_scaf_60908-4.14) and potential E3 ubiquitin ligase RNF213 (Bpl_scaf_25983-1.26,
335 Bpl_scaf_1894-1.45, Supplementary Fig. S10), which were apoptosis suppressor or regulator,
336 were up-regulated[91]. These results suggest that starved bacteriocytes were carrying out cell-
337 type-specific adjustments to cope with stresses. The E3 ubiquitin ligases could also work as in-
338 tracellular immune sensors of bacterial lipopolysaccharides[92]. Thus, the encoded protein may
339 be able to active downstream immunological toolkit to digest the symbiont population for nu-
340 trients.
341 As mentioned above, bacteriocytes obtain nutrients from endosymbionts. KEGG pathway
342 analyses suggested that phagosome, lysosome-related pathways were upregulated in the star-
343 vation state, indicating that bacteriocytes were actively digesting the endosymbionts in the
344 starved *G. platifrons*. Interestingly, protein synthesis activity was more activated in inter lamina
345 cells and VEPCs as supported by the up-regulation of genes encoding ribosomal proteins in both
346 cell populations (Supplementary Tables S6 and S17). This was contrary to the situation in bacte-
347 riocytes and may be a consequence of the high activity of "farming" in bacteriocytes.
348 We anticipated that after moving the starved *G. platifrons* back to Fanmao site, bacterio-
349 cytes and their endosymbionts would "reconstitute" leading to the partly restored "farming"
350 and "milking" pathways. This was confirmed by higher expression of fatty acid metabolic genes

351 in the mussels in the reconstitution state than those in the starvation state, such as long-chain-
352 fatty-acid-ligase ACSBG2-like (Bpl_scaf_28862-1.5), elongation of very long-chain fatty acids 7-
353 like (Bpl_scaf_5959-1.9), and fatty acid desaturase 1-like (Bpl_scaf_35916-0.6). These findings
354 were also consistent with the result of KEGG analyses. The mitochondrial trifunctional enzyme
355 (Bpl_scaf_42376-0.5) was also highly expressed, suggesting a high level of energy-producing
356 activity. The KEGG analyses showed that glutamatergic synthase was enriched in the reconstitu-
357 tion state in comparison with those in both the Fanmao and starvation states. In the insect
358 aphid–Buchnera endosymbiosis model, the host-produced glutamate could be transported and
359 directly utilised by the symbiont[93]. Similar glutamate-based host–symbiont metabolic interac-
360 tion mechanisms were also proposed in the deep-sea mussel *Bathymodiolus thermophilus* and
361 *B. azoricus*[64,94]. As the pseudotime analyses showed above (Fig. 6C), reconstitution was the in-
362 termediate state between Fanmao and starvation. Metabolic and gene regulatory functions of
363 bacteriocytes were still different from that in Fanmao. The KEGG analyses suggested regulatory
364 (Rap1 signalling, retrograde endocannabinoid signalling, chemokine signalling, glucagon signal-
365 ling, thyroid hormone synthesis, mRNA surveillance pathway, etc.) and metabolic pathways
366 were enriched in the reconstitution state (fatty acid metabolism, salivary secretion, aldosterone
367 synthesis and section, insulin secretion and pancreatic section) (Supplementary Fig. S8C). For
368 example, we detected up-regulation of the genes encoding carbonic anhydrases
369 (Bpl_scaf_33596-7.3 and Bpl_scaf_48274-0.3), electroneutral sodium bicarbonate exchanger 1
370 (Bpl_scaf_61230-5.11), and globin-like proteins (Bpl_scaf_50392-1.14 and Bpl_scaf_24370-0.5),
371 which could provide the symbiont with carbon dioxide and oxygen necessary for the symbiont's
372 chemosynthetic metabolism[84,95].
373
374 **5. Summary and outlook:**
375 Using the deep-sea mussel *G. platifrons* as a model organism, we demonstrated the power
376 of integrating snRNA-seq and WISH data in unravelling the mechanism behind animal-microbe
377 symbiosis. The robustness of this strategy showed stable and highly distinguishable expression
378 patterns of each cell type regardless of the different environmental states. We successfully pro-
379 filed the specific roles of different types of cells, including the previously unknown cell types, in

380 maintaining the structure and function of the gill. The supportive cells that located in between
381 (inter lamina cells) and on the basal membrane's surface (BMC1 and BMC2) helped maintain
382 the anatomical structure of the basal membrane. Ciliary and smooth muscle cells involved in gill
383 slice contraction and cilium beat allowing the gathering of material and information from the
384 surrounding environment. Proliferation cells (PBEZCs, DEPCs and VEPCs) gave rise to new cells,
385 including bacteriocytes which obtained nutrients from endosymbionts using intracellular vacu-
386 oles and lysosomes.

387 The snRNA analyses also revealed that different cell types collaborated to support bacterio-
388 cytes' functionality. The PBEZCs gave rise to new bacteriocytes that allowed symbiont colonisa-
389 tion. Bacteriocytes attached to the basal membrane and were stabilised by supportive cells.
390 Mucus cells co-localise with bacteriocytes and help to maintain immune homeostasis. The beat-
391 ing ciliary cells controlled the water flow, providing bacteriocytes with necessary inorganic sub-
392 stances from the environment. This new information on cell-cell interaction certainly advanced
393 our overall understanding of how endosymbiotic microbes and host cells communicate and col-
394 laborate, which cannot be easily achieved through other methods.

395 Moreover, the analysis of snRNA data from bacteriocytes has provided insight into the mo-
396 lecular mechanisms employed by the host to maintain and regulate the symbiosis. Notably, the
397 bacteriocytes-enriched transcripts involved in harbouring, digesting symbionts, and transport-
398 ing nutrients produced by the symbionts were identify and characterised. Our *in situ* transplant
399 experiments by moving mussels between methane-rich and methane-limited sites also pro-
400 vided clues of cell-type specific responses to environmental change. Under a methane-limited
401 environment, the staved mussels more actively consumed endosymbionts through the "farm-
402 ing" pathway. After being moved back to the methane-rich environment, mussels produced
403 more glutamates which sustained the regrowth of symbionts. These preliminary findings
404 showed that the deep-sea mussels were able to control their endosymbionts using a set of
405 genes in response to environmental change. Due to the limitation of remotely operated vehicle
406 (ROV) dives and sampling capacity, we had to have pooled samples of each state for nuclei ex-
407 traction and sequencing. Thus, the cells per cluster could be considered as technical than bio-
408 logical replicates. Although this sampling process strategy has been broadly used in

snRNA/scRNA sequencing[96], we recognise the possible violation of assumptions in *p*-value calculation for DEGs between the three states.

Overall, the single-cell spatial and functional atlas developed in the present work will decipher some common principles of symbiosis and environmental adaption mechanisms of animals. The workflow developed in the present study could provide insightful references for researchers focusing on the mechanistic study of the biological adaptation of biologically and ecologically important non-model animals.

Acknowledgements: This study was supported by the Science and Technology Innovation Project of Laoshan Laboratory (Project Number No. LSKJ202203104), the National Natural Science Foundation of China (Grant No. 42030407), Southern Marine Science and Engineering Guangdong Laboratory (Guangzhou)(HJ202101, SMSEGL20SC01), Major Project of Basic and Applied Basic Research of Guangdong Province (2019B030302004), the Research Grants Council of Hong Kong (C6026-19G-A and 16101822) and the Guangdong Natural Science Funds for Distinguished Young Scholar (2022B1515020033). We appreciate all the assistance provided by the crew of *R/V* 'Kexue' and the operation team of ROV 'Faxian'.

Author contributions: W.H., K.C., P.Y.Q. and L.C.L designed the study. Z.H., L. Cao, Z.Z.S., L. Chao and W.M.X conducted the *in situ* transplant experiments and collected the samples; Z.Q.Y. and W.H. constructed the snRNA-seq library. H.K. performed the bioinformatics analysis. W.H., Z.H., L. Cao, J.L., H.C. and L.Z. performed the experiments. This paper was written by W.H., H.K., K.C., P.Y.Q. and L.C.L. All authors revised the manuscript. All authors read, approved, and contributed to the final manuscript.

Competing interests: The authors declare no competing interests.

Figure legends

Figure 1: Identification of 14 cell types in the gill of deep-sea symbiotic mussel *Gigantidas platifrons*. A: Overall experimental scheme describing the deep-sea *in situ* transplant experiment, the sample preparation procedures and the single-cell analysis and validation pipeline. Three *G. platifrons* samples were included in the present study: 'Fanmao,' Starvation and Reconstitution. The cell nucleus was extracted from each sample, which included a pool of gill posterior tip of three mussels. The snRNA-seq libraries were constructed according to the BD Rhapsody single-nuclei 3′ protocol. Cell population-specific markers were validated by WISH and ISH. B: The image shows the posterior end of the gill of *G. platifrons*. C: UMAP representation of *G. platifrons* gill single cells. Cell clusters are coloured and distinctively labelled. D: Heat map profile of markers in each cluster. The colour gradient represents the expression level of every single cell.

Figure 2: Supportive cell populations of *G. platifrons* gill. A: UMAP representation of the four supportive cell populations. B: Expression profiles of the cell markers that are specific or enriched in the supportive cell populations. The sizes of the circles represent the percentages of cells in those clusters that expressed a specific gene. Genes shown in red were validated by WISH or double FISH. C and C': Schematics demonstrating the overall structural (panel C) and supportive cell distribution (C'). D, F, H, and J: WISH characterisation of the selected representative cell population markers. E, G, I, and K: Double FISH characterisation of the selected representative cell population markers. The white arrowheads in G indicate the BMC1 cells locates at the otter rim of gill slice. Scale bar: 50µm.

Figure 3: Ciliary cell populations of *G. platifrons* gill. A: UMAP representation of the four ciliary cell populations and potential smooth muscle cell population. B: Expression profiles of the cell markers that are specific or enriched in the ciliary cell populations. The sizes of the circles represent the percentages of cells in those clusters that expressed a specific gene. The genes shown in red were validated by WISH or double FISH. C-E, G and I-J: WISH characterisation of the selected representative cell population markers. F and H: SEM analysis of the ciliary cells of *G. platifrons* gill. K: Schematic of the water flow agitated by different ciliary cell types. The

464 coluor of arrowheads corresponds to water flow potentially influenced by specific types of cilia,
465 as indicated by their colour code in Figure 3A.
466
467 **Figure 4:** Proliferation cell populations of *G. platifrons* gill. A: UMAP representation of the three
468 proliferation cell populations. B: Expression profiles of the cell markers that are specific or en-
469 riched in the supportive cell populations. The sizes of the circles represent the percentages of
470 cells in those clusters that expressed a specific gene. Genes shown in red were validated by
471 WISH or double FISH. C and D: Photographic and schematic analyses of the spatial position of
472 the three Proliferation cell populations. E, F and J: FISH and WISH characterisation of the se-
473 lected population markers. The marker genes confirmed by ISH or WISH in the current study are
474 indicated in red. Scale bar: 50 µm.
475
476 **Figure 5:** Characterisation of the bacteriocytes of *G. platifrons*. A: Schematic of the overall
477 structure of *G. platifrons* gill filaments. B: Whole-mount FISH analyses of the overall distribution
478 of bacteriocytes on the *G. platifrons* gill filament. C: SEM analysis of the bacteriocytes. D: TEM
479 analysis of a bacteriocyte. E: UMAP representation of *G. platifrons* bacteriocytes. F: Expression
480 profiles of the cell markers that are specific or enriched in the bacteriocytes. The sizes of the
481 circles represent the percentages of cells in those clusters that expressed a specific gene. Dou-
482 ble FISH validated the genes shown in red. I: Schematic of the host-symbiont interaction based
483 on the single-cell transcriptome of *G. platifrons* bacteriocytes. The marker genes confirmed by
484 ISH in the current study are indicated in red. Scale bar in panel G and H: 25 µm.
485
486 **Figure 6:** Analysis of cell population-specific DEGs. A: UMAP representation of the impact of
487 deep-sea *in situ* transplant treatments on the gene expression pattern of each cell population.
488 The cells from different treatments were labelled with different colours. The dashed line encir-
489 cled bacteriocyte populations have a considerably altered expression profile. B: Histogram of
490 cross-state distances between the centroids of the Fanmao, Starvation and Reconstitution
491 groups per cell type on UMAP. The black dashed lines indicate the bacteriocyte populations
492 whose expression profile was remarkably altered. C: Visualization of bacteriocytes onto the

493 pseudo time map using monocle. The black lines indicate the main path of the pseudotime or-
494 dering of the cells. D: Bifurcation of selected gene expression along two branches in response to
495 environmental perturbation. Genes are clustered hierarchically into two groups, illustrating up-
496 (cluster 1) and down- (cluster2) regulated genes in the starvation state compared with Fanmao.
497 Genes in red colour were discussed in Section 4. The heat map showing the gene expression
498 profiles of all bacteriocytes' DEGs is shown in supplementary Fig. S7; E: Proposed model for the
499 molecular mechanisms of host-symbiont interactions in response to environmental changes.
500
501

502 Materials and methods:

503 **Deep-sea *in situ* transplant experiment and sample collection:** *In situ* transplant experiment
504 was conducted at the 'F-site' cold seep during the R/V 'Kexue' 2020 South China Sea cold seep
505 cruise. The overall design of the *in situ* transplant experiment and environmental states are
506 shown in Figure 1. First, mussels in the methane-rich 'Fanmao' site (meaning 'prosperous' site,
507 22° 06′ 55.425″ N,119° 17′ 08.287″ E, depth 1117m) were scoped into three nylon bags
508 with approximately 10 mussels in each bag. Then, two bags of mussels were transplanted to the
509 low methane Starvation site (Figure 1, 22° 07′ 00″ N, 119° 17′ 07.02″ E, depth 1147.42m).
510 After 11 days of transplantation, one bag of mussels in the Starvation site was moved back to
511 the 'Fanmao' site. On the 14th day of the transplant, three bags of mussels: one bag from the
512 Fanmao site (designated as the 'Fanmao' sample), one bag from the starvation site (designated
513 as the 'Starvation' sample) and one bag of mussels which were first transplanted to the Starva-
514 tion site for 11 days and moved back to the Fanmao site for 3 days (designated as the 'Reconsti-
515 tution' sample) were all retrieved by ROV Fanxian. The mussels were kept in a hydraulic pres-
516 sure-sealed biobox during the ascending of the ROV. The biobox is made of heat-insulated ma-
517 terial, which will prohibit heat exchange with warm surface water. The samples were immedi-
518 ately processed once onboard R/V Kexue. For snRNA-seq, the posterior end tip of the mussel's
519 gill was dissected (Figure 1C), snap-frozen with liquid nitrogen and then stored at −80 °C until
520 use. For WISH, ISH and FISH, the gills of the mussels were first fixed with 4% paraformaldehyde
521 (PFA, prepared with autoclaved 0.22 µM membrane filtered *in situ* seawater) at 4 °C overnight.

522 Then, the gill was washed with ice-cold 1× PBS three times, dehydrated and stored in 100%
523 methanol at −20 °C.
524
525 **Single-nucleus RNA-sequencing of *G. platifrons*:** The gill nucleus was extracted using the Nuclei
526 PURE prep nuclei isolation kit (Sigma-Aldrich). For each sample, posterior end tips from 3 indi-
527 vidual mussels were randomly selected and pooled together. The posterior tips were homoge-
528 nised in 10 mL of ice-cold lysis solution (Nuclei PURE lysis buffer with 0.1% Triton X100 and 1
529 mM DTT) on ice. The cell nuclei were then separated by sucrose gradient centrifugation accord-
530 ing to the manufacturer's protocol. The cell nuclei pellets were washed by re-suspending in ice-
531 cold DPBS–BSA solution (1× DPBS, 0.04% nuclease-free BSA, 0.01% RNase inhibitor; Takara).
532 The nucleus was spun down by centrifugation at 500×g for 5 min at 4 °C. This step was repeated
533 to remove the contaminants from the cell plasma. Finally, the nucleus was re-suspended in the
534 DPBS–BSA solution. The concentration of the cell nucleus was counted by Cell Countess II. Sin-
535 gle-nucleus RNA-seq libraries were then constructed with the BD Rhapsody™ single-cell analysis
536 system using the BD Rhapsody WTA Amplification Kit according to the manufacturer's protocol.
537 The library was subjected to 150bp paired-end sequencing using the Illumina HiSeq 4000 plat-
538 form. The clean reads of three datasets were submitted to the National Centre for Biotechnol-
539 ogy Information Sequence Read Archive database (Bioproject: PRJNA779258).
540
541 **Bioinformatics:** The three raw datasets (Fanmao, Starvation, and Reconstitution) were proc-
542 essed individually following the BD single-cell genomics analysis setup user guide (Doc ID:
543 47383 Rev. 8.0) and BD single-cell genomics bioinformatics handbook (Doc ID: 54169 Rev. 7.0).
544 This process involved the preparation of gene names, alignment of data to the genome, and
545 generation of an expression matrix for each dataset. A *G. platifrons* genome reference v1.0
546 (available at the Dryad Digital Repository; http://dx.doi.org/10.5061/dryad.h9942) was utilized.
547 The genome was indexed and constructed using STAR 2.5.2b[97]. Subsequently, the sequencing
548 data was mapped to the indexed genome using the BD Rhapsody single-nucleus pipeline v1.9,
549 employing default parameters.

550 Each data matrix was converted to a SingleCellExperiment data format, and empty barcodes
551 were removed using the emptyDrops function of DropletUtils v3.14[98]. Then, we converted and
552 processed the data in Seurat v3[28]. We removed cells that had <100 or > 2500 genes and <100
553 or > 6000 unique molecular identifiers (UMIs). We also removed genes that had <10 UMIs in
554 each data matrix. Then, we log-normalised the data and used DoubletFinder v2.0[99] to remove
555 potential doublet, assuming a 7.5% doublet formation rate. The numbers of retained nuclei
556 were 9717, 21614 and 28928 for Fanmao, Starvation and Reconstitution data, respectively
557 (Supplementary Table S20). We used the top 3000 highly variable genes for principal compo-
558 nent analysis (PCA) and a reciprocal PCA approach to integrating the three datasets[100]. The first
559 40 principal components (PCs) were used for uniform manifold approximation and projection
560 (UMAP) dimensional reduction and following clustering (Supplementary Fig. S11). We em-
561 ployed an empirical parameter - a resolution of 0.2 - in the FindClusters function, utilizing the
562 original Louvain algorithm. To identify unique marker genes associated with each cluster, we
563 utilized the FindAllMarkers function from the Seurat package. This analysis employed the Wil-
564 coxon rank sum test, focusing on genes that demonstrated a minimum 0.3-fold difference be-
565 tween two groups of cells. The annotation of cell types relied on the reference of previously
566 published marker genes. In instances where clusters exhibited marker genes that couldn't be
567 associated with known cell types, we pursued the validation process through whole-mount *in*
568 *situ* hybridization (WISH; elaborated below), discerning cell types based on gene expression
569 patterns and morphological characteristics. When WISH displayed uniform expression of
570 marker genes from different clusters within the same cell type, we consolidated those clusters
571 into a single cell type. We assigned cells to 14 reliable cell types (Supplementary Fig. S11). Sup-
572 plementary data S1 presents the counting matrix and Supplementary data S1 presents the av-
573 erage expression of each gene per cell type. To evaluate the stability of each cell type, we im-
574 plemented a bootstrap sampling and clustering strategy comprising 100 iterations using cells
575 combined from all three samples and individual samples[101]. The determination of marker genes
576 per cell type followed the previously described methodology. The identified marker genes were
577 subsequently utilized in KEGG enrichment analysis, employing ClusterProfiler v4.2[102].
578

579 **Cell trajectory analysis:** We conducted slingshot trajectory analyses using Slingshot[103] v2.2.1
580 for a subset of clusters (intercalary cells, dorsal-end proliferation cells,ventral-end proliferation
581 cells, mucus cells, basal membrane cells 1, basal membrane cells 2 and bacteriocytes) to ex-
582 plore the developmental trajectory of cells, assuming that all these cells were developed from
583 the same precursor ('posterior-end budding zone'). We performed PCA for the subsampled data
584 set and conducted dimensional reduction using phateR v1.0.7 for slingshot analyses. We used
585 the Potential of Heat-diffusion for Affinity-based Trajectory Embedding (PHATE) because it
586 could better reveal developmental branches than other tools[104].
587 We also examined the effect of deep-sea transplant experiments on shaping gene expression
588 patterns by comparing the expression levels amongst the three different states of a given clus-
589 ter. We conducted Monocle analyses using Monocle2 and Monocle 3 in R environment[105,106].
590 This comparison was done for the bacteriocytes. The biased number of cells per state could af-
591 fect the results of the dimensional reduction and calculation of marker genes, and the se-
592 quenced nucleus per state was unbalanced; therefore, we first downsampled the cells per clus-
593 ter per state to to a maximum of 1000 nuclei per cell type. Thereafter, we performed PCA and
594 dimensional reduction using UMAP and PHATE, calculated marker genes and conducted sling-
595 shot trajectory and KEGG enrichment analyses as mentioned above for each cell type.
596
597 **Phylogenetic estimation:** Phylogenetic estimation was conducted for E3 ubiquitin ligase
598 RNF213 genes. We downloaded RNF213 genes from GenBank for representative vertebrate and
599 invertebrate species across the tree of life. The amino acid sequences were aligned with the *G.*
600 *platifrons* sequences annotated as E3 ubiquitin ligase (Bpl_scaf_25983-1.26 and Bpl_scaf_1894-
601 1.45) using MAFFT v7.450. The alignment was used to estimate a maximum-likelihood best
602 gene tree and to calculate bootstrap values on each node using RAxML v8.2.
603
604 ***G. platifrons* gill fixation and storage:** The gill tissues of *G. platifrons* were dissected within
605 minutes after the ROV, and samples were retrieved on board R/V Kexue. The gill tissues were
606 briefly washed with ice-cold filtered and autoclaved *in situ* seawater (FAISW) and then fixed in 4%

607 PFA prepared in FAISW at 4 °C overnight. The gill tissues were washed three times with ice-cold
608 PBST, dehydrated in 100% methanol and stored at -20 °C until use.
609
610 **Synthesise probes for mRNA *in situ* hybridisations:** For WISH and double FISH analyses, the
611 DNA fragments (~1000bp) of the targeted genes were first PCR amplified with gene-specific
612 primers (GSPs) pairs using *G. platifrons* gill cDNA as template (the sequences of targeted genes
613 and gene-specific primers were provided in Supplementary Data S3). The amplified fragments
614 were ligated into the pMD18-simpleT vector (Takara) and transformed into *E. coli*. Individual
615 colonies were picked up, and their plasmids were sequenced to confirm the inserts. The tem-
616 plates for in vitro mRNA transcription were amplified using T7 forward GSP (sense probe con-
617 trol) or Sp6 reversed GSPs (antisense probe) combined with either forward or reversed gene-
618 specific primer. Labelled probes and control probes were generated using digoxigenin (DIG)-12-
619 UTP (Roche) or fluorescein-12-UTP (Roche) according to the protocol described by Thisse[107]
620 with Sp6 and T7 RNA polymerase, respectively.
621
622 **Paraffin embedding and double fluorescent *in situ* hybridisation:** The methanal-dehydrated
623 gill slices were incubated in 100% ethanol, a 1:1 mixture of 100% ethanol and xylene and Xylene
624 twice for 1 h each at RT. The samples were embedded by incubating in Paraplast Plus (Sigma-
625 Aldrich) for 2 h at 65 °C and then cooled down to RT. Sections with 5 µM thickness were cut us-
626 ing a microtome (Leica).
627 For double FISH, sections were dewaxed by incubating in xylene twice, a 1:1 mixture of 100%
628 ethanol and xylene, 100% ethanol twice, 95% ethanol, 85% ethanol and 75% ethanol for 15 min
629 each at RT. The sections were washed with PBST three times for 10 min each and then perme-
630 abilised by 2 µg/mL proteinase K (NEB) in PBST for 15 min at RT. Post-digestion fixation was
631 conducted by incubating the sections in 4% PFA in PBST for 30 min at RT. The sections were
632 washed three times with PBST for 15 min each. Pre-hybridisation was conducted by incubating
633 the sections in HM for 1 h at 55 °C. Then, the *in situ* hybridisation was performed by incubating
634 the sections in ~0.5 ng/µL fluorescein (Roche)-labelled probed prepared in fresh HM overnight

635 at 55 °C. The sections were washed three times with 2×SSC for 15 min each at 55 °C, cooled
636 down to room temperature and washed three times with PBST.
637 A second-round hybridisation was conducted on the DIG-labelled oligonucleotides to label the
638 symbiont. The slices were hybridised for 1 h at 46 °C with 100 ng DIG-labelled *G. platifrons*
639 symbiont-specific probe in FISH buffer (0.9 M NaCl, 0.02 M Tris-HCl, 0.01% sodium dodecyl sul-
640 phate [SDS] and 30% formamide). The slices were then washed with FISH washing buffer (0.1 M
641 NaCl, 0.02 M Tris HCl, 0.01% SDS and 5 mM EDTA) three times at 5 min each at 48 °C. The slices
642 were washed with PBST three times and then blocked with blocking buffer (2.5% sheep serum
643 and 2% BSA in sheep serum) for 1 h at room temperature.
644 The slices were then incubated with 1:1000 diluted anti-fluorescein–peroxidase (POD) (Roche)
645 overnight at 4 °C, then washed six times with PBST for 15 min each and three times with TNT
646 buffer (100 mM Tris-HCl, pH 7.5; 100 mM NaCl; 0.1% Tween 20) for 15 min each. Afterwards,
647 the fluorescent signal of the *G. platifrons* gene expression pattern was developed by the TSA
648 fluorescein kit (Akoya Biosciences) according to the manufacturer's protocol. The slices were
649 washed three times, and the remaining POD activity was quenched by incubation in 1% hydro-
650 gen peroxide solution for 1 h at room temperature. Then, the slices were washed three times
651 with PBS, blocked with blocking buffer for 30 min at room temperature, incubated with 1:2500
652 diluted anti-DIG–POD (Roche) for 2 h at RT and washed with PBST for six times and TNT for
653 three times. The symbiont FISH signal was developed using the TSA Cy3 kit (Akoya Biosciences).
654 Finally, the slices were washed with PBST, stained with DAPI, and mounted with ProLong Dia-
655 mond Antifade Mountant (Thermo Fisher).
656
657 **Whole-mount *in situ* hybridisation:** For WISH, the connective region at the end of the W-
658 shaped gill filament was cut off, and each gill slice was carefully peeled off with fine-tip tweez-
659 ers. We dissected gill tissues from 5 individual mussels and pooled all the gill slices together.
660 The gill slices were then rehydrated in 75%, 50% and 25% methanol-PBST (1×PBS with 0.1%
661 Tween 20) for 15 min each, followed by 3×5 min PBST washes. The gill slices were then perme-
662 abilised with 2 µg/mL proteinase K in PBST for 30 min at 37 °C. Post-digestion fixation was con-
663 ducted by fixing the gill slices with 4% PFA in PBST for 30 min at room temperature (RT). After

664 3×5 min PBST wash to remove the residual fixative, the gill slices were pre-hybridised with a
665 hybridisation mix (HM; containing 50% formamide, 5×saline–sodium citrate (SSC), 0.1% Tween
666 20, 10 µg/mL heparin, 500 µg/mL yeast tRNA) for 1 h at 65 °C. For each hybridisation, 5-10 gill
667 slices were added to 400 µL of fresh HM containing ~0.5 ng/µL DIG-labelled probe. Hybridisa-
668 tion was conducted in a 55 °C shaking water bath overnight. Post-hybridisation washes were
669 performed according to the following steps: the gill slices were first washed 3×15 min with hy-
670 bridisation washing buffer (50% formamide, 5×SSC, 0.1% Tween 20), followed by 3×15 min
671 2×SSC with 0.1% Tween 20 and 3×15 min 0.2×SSC with 0.1% Tween 20. The washings were also
672 conducted in a shaking water batch, and all the washing buffers were pre-heated to 55 °C. The
673 samples were washed three times with PBST and then blocked in blocking buffer (2.5% sheep
674 serum, 2% BSA in PBST) for 1 h at RT. Each sample was incubated with 1:10,000 diluted anti-
675 DIG-AP antibody (Roche) at 4 °C overnight. The samples were incubated with the antibody, then
676 washed for 6×15 min with PBST, followed by washing in 3×15 min alkaline Tris buffer (100 mM
677 Tris-HCl, pH 9.5; 100 mM NaCl; 50 mM $MgCl_2$). The samples were incubated in nitro blue tetra-
678 zolium/5-Bromo-4-chloro-3-indolyl phosphate staining solution (Sangon). After the desired ex-
679 pression pattern was revealed, the staining reaction was stopped by 3×15 min PBST–EDTA wash
680 (PBST, 1 mM ETDA). The gill slices were cleared by incubating in 100% glycerol overnight at 4 °C
681 and then mounted on glass slides. The results of control hybridisations (with sense probes)
682 were provided in Supplementary Fig. S13-S16. WISH analyses were repeated with another
683 batch of *G. platifrons* gill slices samples collected during the *R/V* 'Kexue' 2017 South China Sea
684 cold seep cruise to confirm the consistency in expression patterns.
685
686
687 **Microscopy imaging:** All the WISH samples and whole-mount 16S FISH images were observed
688 and imaged with a Nikon Eclipse Ni microscope with a DS-Ri2 camera. The double FISH slides
689 were imaged with a Zeiss LSM710 confocal microscope.
690
691 **Electron microscopy analysis:** The gill slices of the *G. platifrons* were dissected and fixed in
692 electron microscopy fixative (2.5% glutaraldehyde and 2% PFA) at 4 °C. For SEM analysis, the

samples were dehydrated in a graded ethanol series and then dried at the critical point. The samples were then coated with gold (sputter/carbon Thread, EM ACE200) and observed under a scanning electron microscope (VEGA3, Tescan). For TEM analysis, the samples were rinsed with double distilled water, post-fixed with 1% osmium tetroxide and then washed with double distilled water. The samples were then rinsed, dehydrated and embedded in Ep812 resin. Ultra-thin sections were obtained with an ultramicrotome (70 nm thickness, Reichert-Jung Ultracut E). The sections were then double-stained with lead citrate and uranyl acetate. The cells were observed under a transmission electron microscope (JEM1200, Jeol) operated under 100 kV.

701 **References**

702 1 Kremer, N. *et al.* Initial symbiont contact orchestrates host-organ-wide transcriptional
703 changes that prime tissue colonization. *Cell Host & Microbe.* **14**, 183-194 (2013).
704 https://doi.org:10.1016/j.chom.2013.07.006
705 2 Bang, C. *et al.* Metaorganisms in extreme environments: do microbes play a role in
706 organismal adaptation? *Zoology (Jena)* (2018). https://doi.org:10.1016/j.zool.2018.02.004
707 3 Franke, M., Geier, B., Hammel, J. U., Dubilier, N. & Leisch, N. Coming together-symbiont
708 acquisition and early development in deep-sea bathymodioline mussels. *Proc. R. Soc.* **288**,
709 20211044 (2021). https://doi.org:10.1098/rspb.2021.1044
710 4 Dubilier, N., Bergin, C. & Lott, C. Symbiotic diversity in marine animals: the art of
711 harnessing chemosynthesis. *Nat. Rev. Microbiol.* **6**, 725 (2008).
712 https://doi.org:10.1038/nrmicro1992
713 5 Sogin, E. M., Kleiner, M., Borowski, C., Gruber-Vodicka, H. R. & Dubilier, N. Life in the dark:
714 phylogenetic and physiological diversity of chemosynthetic symbioses. *Annu. Rev.*
715 *Microbiol.* **75**, 695-718 (2021). https://doi.org:10.1146/annurev-micro-051021-123130
716 6 Xu, T., Feng, D., Tao, J. & Qiu, J.-W. A new species of deep-sea mussel (Bivalvia: Mytilidae:
717 *Gigantidas*) from the South China Sea: Morphology, phylogenetic position, and gill-
718 associated microbes. *Deep Sea Res. Part I Oceanogr. Res. Pap.* **146**, 79-90 (2019).
719 https://doi.org:https://doi.org/10.1016/j.dsr.2019.03.001
720 7 DeChaine, E. G. & Cavanaugh, C. M. Symbioses of methanotrophs and deep-sea mussels
721 (Mytilidae: Bathymodiolinae). *Prog. Mol. Subcell. Biol.* **41**, 227-249 (2006).
722 https://doi.org:10.1007/3-540-28221-1_11
723 8 Fujiwara, Y. *et al.* Phylogenetic characterization of endosymbionts in three hydrothermal
724 vent mussels influence on host distributions. *Mar. Ecol. Prog. Ser.* **208**, 147-155 (2000).
725 https://doi:10.3354/meps208147
726 9 Kiel, S. The vent and seep biota : aspects from microbes to ecosystems. (Springer, 2010).
727 https://doi.org/10.1007/978-90-481-9572-5
728 10 Vrijenhoek, R. C. Genetic diversity and connectivity of deep-sea hydrothermal vent
729 metapopulations. *Mol. Ecol.* **19**, 4391-4411 (2010). https://doi.org:10.1111/j.1365-
730 294X.2010.04789.x
731 11 Halary, S., Riou, V., Gaill, F., Boudier, T. & Duperron, S. 3D FISH for the quantification of
732 methane- and sulphur-oxidizing endosymbionts in bacteriocytes of the hydrothermal vent
733 mussel *Bathymodiolus azoricus*. *ISME J* **2**, 284-292 (2008).
734 https://doi.org:10.1038/ismej.2008.3
735 12 Zheng, P. *et al.* Insights into deep-sea adaptations and host-symbiont interactions: A
736 comparative transcriptome study on Bathymodiolus mussels and their coastal relatives.
737 *Mol. Ecol.* **26**, 5133-5148 (2017). https://doi.org:10.1111/mec.14160
738 13 Fiala-Médioni, A., Métivier, C., Herry, A. & Le Pennec, M. *Ultrastructure of the gill of the*
739 *hydrothermal-vent mytilid Bathymodiolus sp.*. *Mar. Biol.* **92**, 65–72 (1986).
740 https://doi.org/10.1007/BF00392747
741 14 Wong, Y. H. *et al.* High-throughput transcriptome sequencing of the cold seep mussel
742 Bathymodiolus platifrons. *Sci. Rep.* **5**, 16597 (2015). https://doi.org:10.1038/srep16597

743 15 Sun, J. *et al.* Adaptation to deep-sea chemosynthetic environments as revealed by mussel
744 genomes. *Nat. Ecol. Evol.* **1**, 121 (2017). https://doi.org:10.1038/s41559-017-0121
745 16 Bettencourt, R. *et al.* An Insightful Model to Study Innate Immunity and Stress Response
746 in Deep‐Sea Vent Animals: Profiling the Mussel *Bathymodiolus azoricus*. *Organismal and*
747 *Molecular Malacology*, **8**, (2017). https://doi.org:10.5772/68034.
748 17 Barros, I. *et al.* Post-capture immune gene expression studies in the deep-sea
749 hydrothermal vent mussel *Bathymodiolus azoricus* acclimatized to atmospheric pressure.
750 *Fish Shellfish Immunol* **42**, 159-170 (2015). https://doi.org:10.1016/j.fsi.2014.10.018
751 18 Wang, H. *et al.* Molecular analyses of the gill symbiosis of the bathymodiolin mussel
752 *Gigantidas platifrons*. *iScience* **24**, 101894 (2021).
753 https://doi.org:10.1016/j.isci.2020.101894
754 19 Chen, K. H., Boettiger, A. N., Moffitt, J. R., Wang, S. & Zhuang, X. RNA imaging. Spatially
755 resolved, highly multiplexed RNA profiling in single cells. *Science* **348**, 6090 (2015).
756 https://doi.org:10.1126/science.aaa6090
757 20 Hwang, B., Lee, J. H. & Bang, D. Single-cell RNA sequencing technologies and
758 bioinformatics pipelines. *Exp. Mol. Med.* **50**, 1-14 (2018). https://doi.org:10.1038/s12276-
759 018-0071-8
760 21 Saliba, A. E., Westermann, A. J., Gorski, S. A. & Vogel, J. Single-cell RNA-seq: advances and
761 future challenges. *Nucleic Acids Res* **42**, 8845-8860 (2014).
762 https://doi.org:10.1093/nar/gku555
763 22 Chen, X., Teichmann, S. A. & Meyer, K. B. From tissues to cell types and back: single-cell
764 gene expression analysis of tissue architecture. *Annu. Rev. Biomed. Data Sci.* **1**, 29-51
765 (2018). https://doi.org:10.1146/annurev-biodatasci-080917-013452
766 23 Wu, H., Kirita, Y., Donnelly, E. L. & Humphreys, B. D. Advantages of single-nucleus over
767 single-cell RNA sequencing of adult kidney: rare cell types and novel cell states revealed in
768 fibrosis. *J. Am. Soc. Nephrol.* **30**, 23-32 (2019). https://doi.org:10.1681/ASN.2018090912
769 24 Feng, D. *et al.* Using Bathymodiolus tissue stable carbon, nitrogen and sulfur isotopes to
770 infer biogeochemical process at a cold seep in the South China Sea. *Deep Sea Res. Part I*
771 *Oceanogr. Res.* **104**, 52-59 (2015).
772 https://doi.org:https://doi.org/10.1016/j.dsr.2015.06.011
773 25 Kharchenko, P. V., Silberstein, L. & Scadden, D. T. Bayesian approach to single-cell
774 differential expression analysis. *Nat. Methods.* **11**, 740-742 (2014).
775 https://doi.org:10.1038/nmeth.2967
776 26 Elyanow, R., Dumitrascu, B., Engelhardt, B. E. & Raphael, B. J. netNMF-sc: leveraging gene-
777 gene interactions for imputation and dimensionality reduction in single-cell expression
778 analysis. *Genome. Res.* **30**, 195-204 (2020). https://doi.org:10.1101/gr.251603.119
779 27 Hao, Y. *et al.* Integrated analysis of multimodal single-cell data. *Cell* **184**, 3573-3587
780 (2021). https://doi.org:10.1016/j.cell.2021.04.048
781 28 Stuart, T. *et al.* Comprehensive integration of single-cell data. *Cell* **177**, 1888-1902 (2019).
782 https://doi.org:10.1016/j.cell.2019.05.031
783 29 Petibon, C., Malik Ghulam, M., Catala, M. & Abou Elela, S. Regulation of ribosomal protein
784 genes: An ordered anarchy. *WIREs RNA* **12**, e1632 (2021).
785 https://doi.org:https://doi.org/10.1002/wrna.1632

786 30 Welcker, D. *et al.* Hemicentin-1 is an essential extracellular matrix component of the
787 dermal–epidermal and myotendinous junctions. *Sci. Rep.* **11**, 17926 (2021).
788 https://doi.org:10.1038/s41598-021-96824-4
789 31 Dufour, S. C. & Beninger, P. G. A functional interpretation of cilia and mucocyte
790 distributions on the abfrontal surface of bivalve gills. *Mar. Biol.* **138**, 295-309 (2001).
791 https://doi.org:10.1007/s002270000466
792 32 Dufour, S. C. Gill anatomy and the evolution of symbiosis in the bivalve family Thyasiridae.
793 *Biol. Bull.* **208**, 200-212 (2005). https://doi.org:10.2307/3593152
794 33 Gómez-Mendikute, A., Elizondo, M., Venier, P. & Cajaraville, M. P. Characterization of
795 mussel gill cells in vivo and in vitro. *Cell Tissue Res.* **321**, 131-140 (2005).
796 https://doi.org:10.1007/s00441-005-1093-9
797 34 Beninger, P. G. & Dufour, S. Mucocyte distribution and relationship to particle transport
798 on the pseudolamellibranch gill of *Crassostrea virginica* (Bivalvia:Ostreidae). *Mar. Ecol.*
799 *Progr. Ser.* **137**, 133-138 (1996). https://doi.org:10.3354/meps137133
800 35 Gerdol, M. *et al.* The C1q domain containing proteins of the Mediterranean mussel
801 Mytilus galloprovincialis: A widespread and diverse family of immune-related molecules.
802 *Dev. Comp. Immunol.* **35**, 635-643 (2011).
803 https://doi.org:https://doi.org/10.1016/j.dci.2011.01.018
804 36 Wang, W., Song, X., Wang, L. & Song, L. Pathogen-derived carbohydrate recognition in
805 molluscs immune defense. *Int. J. Mol. Sci.* **19**, 721 (2018).
806 https://doi.org:10.3390/ijms19030721
807 37 Saco, A., Rey-Campos, M., Novoa, B. & Figueras, A. Transcriptomic response of mussel
808 gills after a *Vibrio splendidus* infection demonstrates their role in the immune response.
809 *Front. Immunol.* **11**, 615580 (2020). https://doi.org:10.3389/fimmu.2020.615580
810 38 Richoux, N. B. & Thompson, R. J. Regulation of particle transport within the ventral groove
811 of the mussel (*Mytilus edulis*) gill in response to environmental conditions. *J. Exp. Mar.*
812 *Biol. Ecol.* **260**, 199-215 (2001). https://doi.org:10.1016/s0022-0981(01)00254-4
813 39 Riisgård, H. U., Egede, P. P. & Barreiro Saavedra, I. Feeding behaviour of the mussel,
814 *Mytilus edulis*: New observations, with a minireview of current knowledge. *J. Mar. Biol.*
815 **2011**, 312459 (2011). https://doi.org:10.1155/2011/312459
816 40 Heude, É., Shaikho, S. & Ekker, M. The dlx5a/dlx6a genes play essential roles in the early
817 development of zebrafish median fin and pectoral structures. *PLOS ONE* **9**, e98505 (2014).
818 https://doi.org:10.1371/journal.pone.0098505
819 41 Han, S. *et al.* TULP3 is required for localization of membrane-associated proteins ARL13B
820 and INPP5E to primary cilia. *Biochem. Biophys. Res. Commun.* **509**, 227-234 (2019).
821 https://doi.org/10.1016/j.bbrc.2018.12.109
822 42 Louka, P. *et al.* Proteins that control the geometry of microtubules at the ends of cilia. *J.*
823 *Cell Biol.* **217**, 4298-4313 (2018). https://doi.org:10.1083/jcb.201804141
824 43 Das, A., Dickinson, D. J., Wood, C. C., Goldstein, B. & Slep, K. C. Crescerin uses a TOG
825 domain array to regulate microtubules in the primary cilium. *Mol. Biol. Cell.* **26**, 4248-
826 4264 (2015). https://doi.org:10.1091/mbc.E15-08-0603
827 44 Llorente-Cortes, V., Martinez-Gonzalez, J. & Badimon, L. LDL receptor-related protein
828 mediates uptake of aggregated LDL in human vascular smooth muscle cells. *Arterioscler.*
829 *Thromb. Vasc. Biol.* **20**, 1572-1579 (2000). https://doi.org:10.1161/01.atv.20.6.1572

45 Chen, X. *et al.* Angiotensin-converting enzyme in smooth muscle cells promotes atherosclerosis-brief report. *Arterioscler. Thromb. Vasc. Biol.* **36**, 1085-1089 (2016). https://doi.org:10.1161/ATVBAHA.115.307038

46 Linke, W. A. & Grützner, A. Pulling single molecules of titin by AFM—recent advances and physiological implications. *Pflug. Arch. Eur.* **456**, 101-115 (2008). https://doi.org:10.1007/s00424-007-0389-x

47 St Paul, A., Corbett, C. B., Okune, R. & Autieri, M. V. Angiotensin II, Hypercholesterolemia, and vascular smooth muscle cells: A perfect trio for vascular pathology. *Int. J. Mol. Sci.* **21** 4525 (2020). https://doi.org:10.3390/ijms21124525

48 Ytrehus, K., Ludvigsen, S., Mancusi, C., Gerdts, E. & de Simone, G. Heart angiotensin-converting enzyme and angiotensin-converting enzyme 2 gene expression associated with male sex and salt-sensitive hypertension in the Dahl Rat. *Front. physiol.* **12** (2021). https://doi.org:10.3389/fphys.2021.663819

49 Keller, T. C., 3rd *et al.* Role of titin in nonmuscle and smooth muscle cells. *Adv. Exp. Med. Biol.* **481**, 265-277 (2000). https://doi.org:10.1007/978-1-4615-4267-4_16

50 Chen, J. V. *et al.* Rootletin organizes the ciliary rootlet to achieve neuron sensory function in *Drosophila*. *J. Cell. Biol.* **211**, 435-453 (2015). https://doi.org:10.1083/jcb.201502032

51 Styczynska-Soczka, K. & Jarman, A. P. The *Drosophila* homologue of rootletin is required for mechanosensory function and ciliary rootlet formation in chordotonal sensory neurons. *Cilia* **4**, 9 (2015). https://doi.org:10.1186/s13630-015-0018-9

52 Mohan, S., Timbers, T. A., Kennedy, J., Blacque, O. E. & Leroux, M. R. Striated rootlet and nonfilamentous forms of rootletin maintain ciliary function. *Curr. Biol.* **23**, 2016-2022 (2013). https://doi.org:10.1016/j.cub.2013.08.033

53 Jones, S. E. & Jomary, C. Secreted Frizzled-related proteins: searching for relationships and patterns. *Bioessays* **24**, 811-820 (2002). https://doi.org:10.1002/bies.10136

54 Gillis, W. Q., Bowerman, B. A. & Schneider, S. Q. The evolution of protostome GATA factors: molecular phylogenetics, synteny, and intron/exon structure reveal orthologous relationships. *BMC Evol. Biol.* **8**, 112-112 (2008). https://doi.org:10.1186/1471-2148-8-112

55 Zhang, Z., Liu, L., Twumasi-Boateng, K., Block, D. H. S. & Shapira, M. FOS-1 functions as a transcriptional activator downstream of the *C. elegans* JNK homolog KGB-1. *Cell. Signal.* **30**, 1-8 (2017). https://doi.org:https://doi.org/10.1016/j.cellsig.2016.11.010

56 Phochanukul, N. & Russell, S. No backbone but lots of Sox: Invertebrate Sox genes. *Int. J. Biochem. Cell Biol.* **42**, 453-464 (2010). https://doi.org:https://doi.org/10.1016/j.biocel.2009.06.013

57 Cannuel, R., Beninger, P. G., McCombie, H. & Boudry, P. Gill Development and its functional and evolutionary implications in the blue mussel *Mytilus edulis* (Bivalvia: Mytilidae). *Biol. Bull.* **217**, 173-188 (2009). https://doi.org:10.1086/BBLv217n2p173

58 Leibson, N. L. & Movchan, O. T. Cambial zones in gills of Bivalvia. *Mar. Biol.* **31**, 175-180 (1975). https://doi.org:10.1007/BF00391629

59 Wentrup, C., Wendeberg, A., Schimak, M., Borowski, C. & Dubilier, N. Forever competent: deep-sea bivalves are colonized by their chemosynthetic symbionts throughout their lifetime. *Environ. Microbiol.* **16**, 3699-3713 (2014). https://doi.org:10.1111/1462-2920.12597

874 60 Mohieldin, A. M. *et al.* Proteomic identification reveals the role of ciliary extracellular-like
875 vesicle in cardiovascular function. *Adv. Sci.* **7**, 1903140 (2020).
876 https://doi.org:https://doi.org/10.1002/advs.201903140
877 61 Neumann, D. & Kappes, H. On the growth of bivalve gills initiated from a lobule-producing
878 budding zone. *Biol. Bull.* **205**, 73-82 (2003). https://doi.org:10.2307/1543447
879 62 Piquet, B. et al. Regionalized cell proliferation in the symbiont-bearing gill of the
880 hydrothermal vent mussel Bathymodiolus azoricus. Symbiosis 82, 225-233 (2020).
881 https://doi.org/10.1007/s13199-020-00720-w
882 63 Streams, M. E., Fisher, C. R. & Fiala-Médioni, A. Methanotrophic symbiont location and
883 fate of carbon incorporated from methane in a hydrocarbon seep mussel. *Mar. Biol.* **129**,
884 465-476 (1997). https://doi.org:10.1007/s002270050187
885 64 Ponnudurai, R. *et al.* Metabolic and physiological interdependencies in the *Bathymodiolus*
886 *azoricus* symbiosis. *ISME J* **11**, 463-477 (2017). https://doi.org:10.1038/ismej.2016.124
887 65 Barry, J. P. *et al.* Methane‐based symbiosis in a mussel, *Bathymodiolus platifrons*, from
888 cold seeps in Sagami Bay, Japan. *Invertebr. Biol.* **121**, 47-54 (2002).
889 https://doi.org:doi:10.1111/j.1744-7410.2002.tb00128.x
890 66 Renoz, F., Noel, C., Errachid, A., Foray, V. & Hance, T. Infection dynamic of symbiotic
891 bacteria in the pea *Aphid acyrthosiphon pisum* gut and host immune response at the early
892 steps in the infection process. *Plos One* **10,** 0122099 (2015).
893 https://doi.org:ARTNe012209910.1371/journal.pone.
894 67 Guan, H. *et al.* Lipid Biomarker Patterns Reflect Nutritional Strategies of Seep-Dwelling
895 Bivalves From the South China Sea. *Front. Mar. Sci.* **9,** 3398 (2022).
896 https://doi.org:10.3389/fmars.2022.831286
897 68 Li, Y. *et al.* Genomic adaptations to chemosymbiosis in the deep-sea seep-dwelling
898 tubeworm *Lamellibrachia luymesi*. *BMC Biol.* **17**, 91 (2019).
899 https://doi.org:10.1186/s12915-019-0713-x
900 69 Sun, Y. *et al.* Genomic signatures supporting the symbiosis and formation of chitinous
901 tube in the deep-sea tubeworm *Paraescarpia echinospica. Mol. Biol. Evol.* **38**, 4116-4134
902 (2021). https://doi.org:10.1093/molbev/msab203
903 70 Takishita, K. *et al.* Genomic evidence that methanotrophic endosymbionts likely provide
904 deep-sea bathymodiolus mussels with a sterol intermediate in cholesterol biosynthesis.
905 *Genome Biol. Evol.* **9**, 1148-1160 (2017). https://doi.org:10.1093/gbe/evx082
906 71 Demidenko, A., Akberdin, I. R., Allemann, M., Allen, E. E. & Kalyuzhnaya, M. G. Fatty acid
907 biosynthesis pathways in *Methylomicrobium buryatense* 5G(B1). *Front. Microbiol.* **7**, 2167
908 (2016). https://doi.org:10.3389/fmicb.2016.02167
909 72 Brasaemle, D. L. *et al.* Adipose differentiation-related protein is an ubiquitously expressed
910 lipid storage droplet-associated protein. *J. Lipid Res.* **38**, 2249-2263 (1997).
911 https://doi.org/10.1016/S0022-2275(20)34939-7
912 73 Cheng, D. *et al.* Expression, purification, and characterization of human and rat acetyl
913 coenzyme A carboxylase (ACC) isozymes. *Protein Expr. Purif.* **51**, 11-21 (2007).
914 https://doi.org:10.1016/j.pep.2006.06.005
915 74 Monroig, Ó. & Kabeya, N. Desaturases and elongases involved in polyunsaturated fatty
916 acid biosynthesis in aquatic invertebrates: a comprehensive review. *Fish. Sci.* **84**, 911-928
917 (2018). https://doi.org:10.1007/s12562-018-1254-x

75 Kabeya, N. et al. Unique fatty acid desaturase capacities uncovered in Hediste diversicolor illustrate the roles of aquatic invertebrates in trophic upgrading. *Philos. Trans. R. Soc.* **375**, 20190654 (2020). https://doi.org:10.1098/rstb.2019.0654

76 Soupene, E. & Kuypers, F. A. Mammalian long-chain acyl-CoA synthetases. *Exp. Biol. Med. (Maywood).* **233**, 507-521 (2008). https://doi.org:10.3181/0710-MR-287

77 Alves-Bezerra, M. *et al.* Long-chain acyl-CoA synthetase 2 knockdown leads to decreased fatty acid oxidation in fat body and reduced reproductive capacity in the insect *Rhodnius prolixus*. *Biochim. Biophys. Acta.* **1861**, 650-662 (2016). https://doi.org:10.1016/j.bbalip.2016.04.007

78 Hoglund, P. J., Nordstrom, K. J. V., Schioth, H. B. & Fredriksson, R. The solute carrier families have a remarkably long evolutionary history with the majority of the human families present before divergence of bilaterian species. *Mol. Biol. Evol.* **28**, 1531-1541 (2011). https://doi.org:10.1093/molbev/msq350

79 Mohamed, A. R. *et al.* Dual RNA-sequencing analyses of a coral and its native symbiont during the establishment of symbiosis. *Mol. Ecol.* **29**, 3921-3937 (2020). https://doi.org:10.1111/mec.15612

80 Bertucci, A., Foret, S., Ball, E. E. & Miller, D. J. Transcriptomic differences between day and night in *Acropora millepora* provide new insights into metabolite exchange and light-enhanced calcification in corals. *Mol. Ecol.* **24**, 4489-4504 (2015). https://doi.org:10.1111/mec.13328

81 Hamada, M. *et al.* Metabolic co-dependence drives the evolutionarily ancient Hydra-Chlorella symbiosis. *Elife* **7,** e35122 (2018). https://doi.org:10.7554/eLife.35122

82 Duncan, R. P., Feng, H., Nguyen, D. M. & Wilson, A. C. Gene family expansions in aphids maintained by endosymbiotic and nonsymbiotic traits. *Genome Biol. Evol.* **8**, 753-764 (2016). https://doi.org:10.1093/gbe/evw020

83 Feng, H. L. *et al.* Trading amino acids at the aphid-Buchnera symbiotic interface. *P. Natl. Acad. Sci. USA.* **116**, 16003-16011 (2019). https://doi.org:10.1073/pnas.1906223116

84 Ip, J. C. *et al.* Host-endosymbiont genome integration in a deep-sea chemosymbiotic clam. *Mol. Biol. Evol.* **38**, 502-518 (2021). https://doi.org:10.1093/molbev/msaa241

85 Hongo, Y. *et al.* Expression of genes involved in the uptake of inorganic carbon in the gill of a deep-sea vesicomyid clam harboring intracellular thioautotrophic bacteria. *Gene* **585**, 228-240 (2016). https://doi.org:https://doi.org/10.1016/j.gene.2016.03.033

86 Sotiriou, S. *et al.* Ascorbic-acid transporter Slc23a1 is essential for vitamin C transport into the brain and for perinatal survival. *Nat. Med.* **8**, 514-517 (2002). https://doi.org:10.1038/0502-514

87 Aydemir, T. B. et al. Zinc transporter ZIP14 functions in hepatic zinc, iron and glucose homeostasis during the innate immune response (endotoxemia). *PLoS One* **7**, e48679 (2012). https://doi.org:10.1371/journal.pone.0048679

88 Turi, Z., Lacey, M., Mistrik, M. & Moudry, P. Impaired ribosome biogenesis: mechanisms and relevance to cancer and aging. Aging (Albany NY) **11**, 2512-2540 (2019). https://doi.org:10.18632/aging.101922

89 Hay, B. A. Understanding IAP function and regulation: a view from Drosophila. Cell. Death. Differ. **7**, 1045-1056 (2000). https://doi.org:10.1038/sj.cdd.4400765

90 Dubrez-Daloz, L., Dupoux, A. & Cartier, J. IAPS : More than just inhibitors of apoptosis proteins. Cell Cycle **7**, 1036-1046 (2008). https://doi.org:10.4161/cc.7.8.5783

91 Pflug, K. M. & Sitcheran, R. Targeting NF-κB-inducing kinase (NIK) in immunity, inflammation, and cancer. *Int. J. Mol. Sci.* **21**, 8470 (2020).

92 Otten, E. G. *et al.* Ubiquitylation of lipopolysaccharide by RNF213 during bacterial infection. *Nature* **594**, 111-116 (2021). https://doi.org:10.1038/s41586-021-03566-4

93 Price, D. R. *et al.* Aphid amino acid transporter regulates glutamine supply to intracellular bacterial symbionts. *Proc. Natl. Acad. Sci. USA.* **111**, 320-325 (2014). https://doi.org:10.1073/pnas.1306068111

94 Ponnudurai, R. *et al.* Comparative proteomics of related symbiotic mussel species reveals high variability of host–symbiont interactions. *ISME J.* **14**, 649-656 (2020). https://doi.org:10.1038/s41396-019-0517-6

95 Tashian, R. E. The carbonic anhydrases: widening perspectives on their evolution, expression and function. *Bioessays* **10**, 186-192 (1989). https://doi.org:10.1002/bies.950100603

96 Hicks, S. C., Townes, F. W., Teng, M. & Irizarry, R. A. Missing data and technical variability in single-cell RNA-sequencing experiments. *Biostatistics* **19**, 562-578 (2017). https://doi.org:10.1093/biostatistics/kxx053

97 Dobin, A. et al. STAR: ultrafast universal RNA-seq aligner. Bioinformatics 29, 15-21 (2013). https://doi.org/10.1093/bioinformatics/bts635

98 Lun, A. T. L. *et al.* EmptyDrops: distinguishing cells from empty droplets in droplet-based single-cell RNA sequencing data. *Genome Biol.* **20**, 63 (2019). https://doi.org:10.1186/s13059-019-1662-y

99 McGinnis, C. S., Murrow, L. M. & Gartner, Z. J. DoubletFinder: Doublet detection in single-cell RNA sequencing data using artificial nearest neighbors. *Cell Systems* **8**, 329-337 (2019). https://doi.org:https://doi.org/10.1016/j.cels.2019.03.003

100 Stuart, T. et al. Comprehensive Integration of Single-Cell Data. *Cell* **177**, 1888-1902.e1821 (2019). https://doi.org:https://doi.org/10.1016/j.cell.2019.05.031

101 Singh, P. & Zhai, Y. Deciphering Hematopoiesis at single cell level through the lens of reduced dimensions. *bioRxiv*, 2022.2006.2007.495099 (2022). https://doi.org:10.1101/2022.06.07.495099

102 Wu, T. et al. clusterProfiler 4.0: A universal enrichment tool for interpreting omics data. *The Innovation* **2**, 100141 (2021). https://doi.org:https://doi.org/10.1016/j.xinn.2021.100141

103 Street, K. et al. Slingshot: cell lineage and pseudotime inference for single-cell transcriptomics. *BMC Genom.* **19**, 477 (2018). https://doi.org:10.1186/s12864-018-4772-0

104 Moon, K. R. et al. Visualizing structure and transitions in high-dimensional biological data. *Nat. Biotechnol.* **37**, 1482-1492 (2019). https://doi.org:10.1038/s41587-019-0336-3

105 Qiu, X. et al. Reversed graph embedding resolves complex single-cell trajectories. Nat Methods 14, 979-982 (2017). https://doi.org/10.1038/nmeth.4402

106 Cao, J. et al. The single-cell transcriptional landscape of mammalian organogenesis. Nature 566, 496-502 (2019). https://doi.org/10.1038/s41586-019-0969-x

107 Thisse, C. & Thisse, B. High-resolution in situ hybridization to whole-mount zebrafish embryos. Nat. Protoc. 3, 59-69 (2008). https://doi.org:10.1038/nprot.2007.514

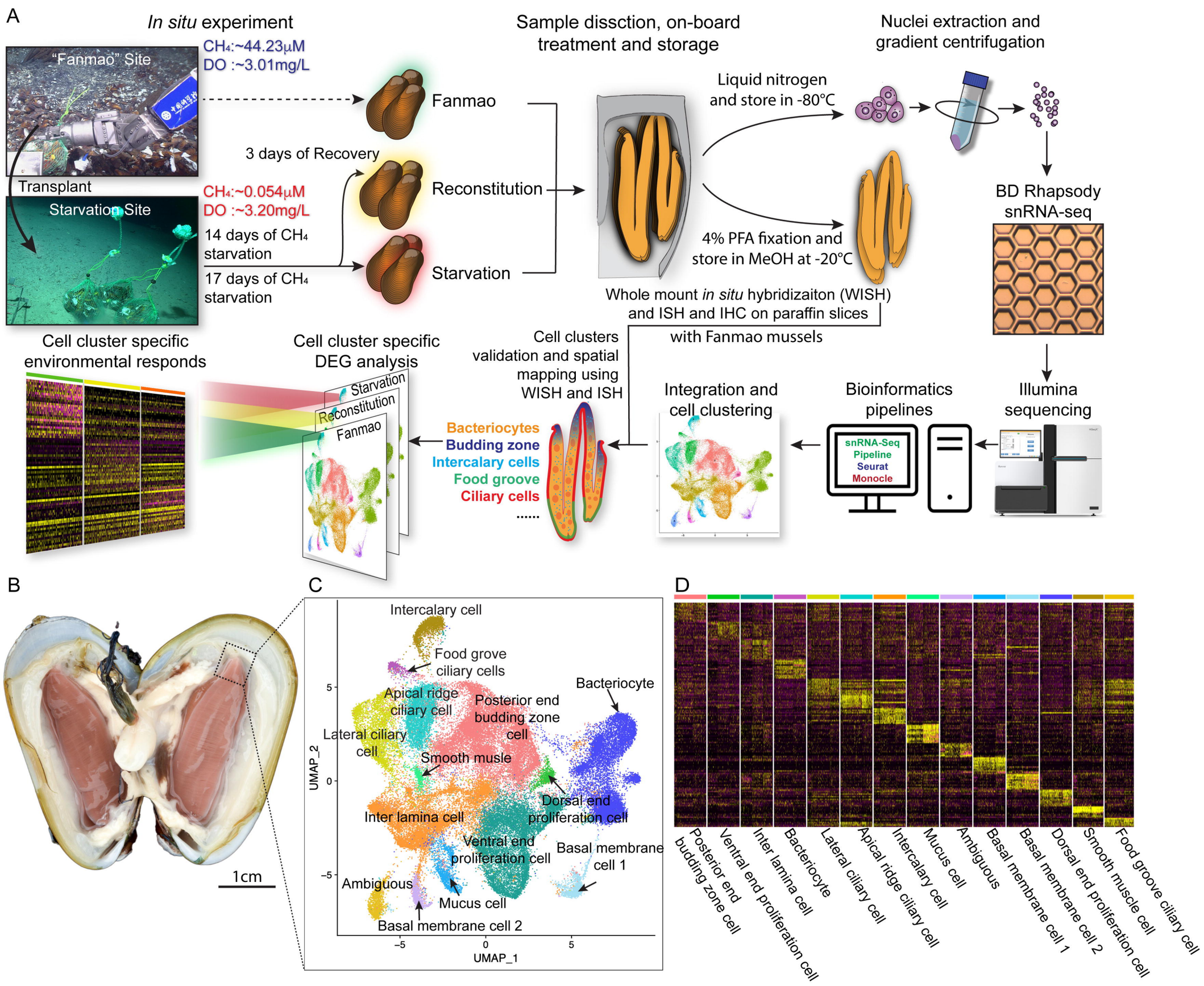
A
In situ experiment
"Fanmao" Site
CH4:~44.23μM
DO :~3.01mg/L
Transplant
Starvation Site
CH4:~0.054μM
DO :~3.20mg/L
14 days of CH4 starvation
17 days of CH4 starvation
3 days of Recovery
Fanmao
Reconstitution
Starvation
Sample dissction, on-board treatment and storage
Liquid nitrogen and store in -80°C
4% PFA fixation and store in MeOH at -20°C
Nuclei extraction and gradient centrifugation
BD Rhapsody snRNA-seq
Illumina sequencing
Bioinformatics pipelines
snRNA-Seq Pipeline Seurat Monocle
Integration and cell clustering
Whole mount in situ hybridizaiton (WISH) and ISH and IHC on paraffin slices with Fanmao mussels
Cell clusters validation and spatial mapping using WISH and ISH
Bacteriocytes
Budding zone
Intercalary cells
Food groove
Ciliary cells
.....
Cell cluster specific DEG analysis
Starvation
Reconstitution
Fanmao
Cell cluster specific environmental responds
B
1cm
C
Intercalary cell
Food grove ciliary cells
Apical ridge ciliary cell
Posterior end budding zone cell
Bacteriocyte
Lateral ciliary cell
Smooth musle
Dorsal end proliferation cell
Inter lamina cell
Ventral end proliferation cell
Basal membrane cell 1
Ambiguous
Mucus cell
Basal membrane cell 2
UMAP_2
UMAP_1
D
Posterior end budding zone cell
Ventral end proliferation cell
Inter lamina cell
Bacteriocyte
Lateral ciliary cell
Apical ridge ciliary cell
Intercalary cell
Mucus cell
Ambiguous
Basal membrane cell 1
Basal membrane cell 2
Dorsal end proliferation cell
Smooth muscle cell
Food groove ciliary cell

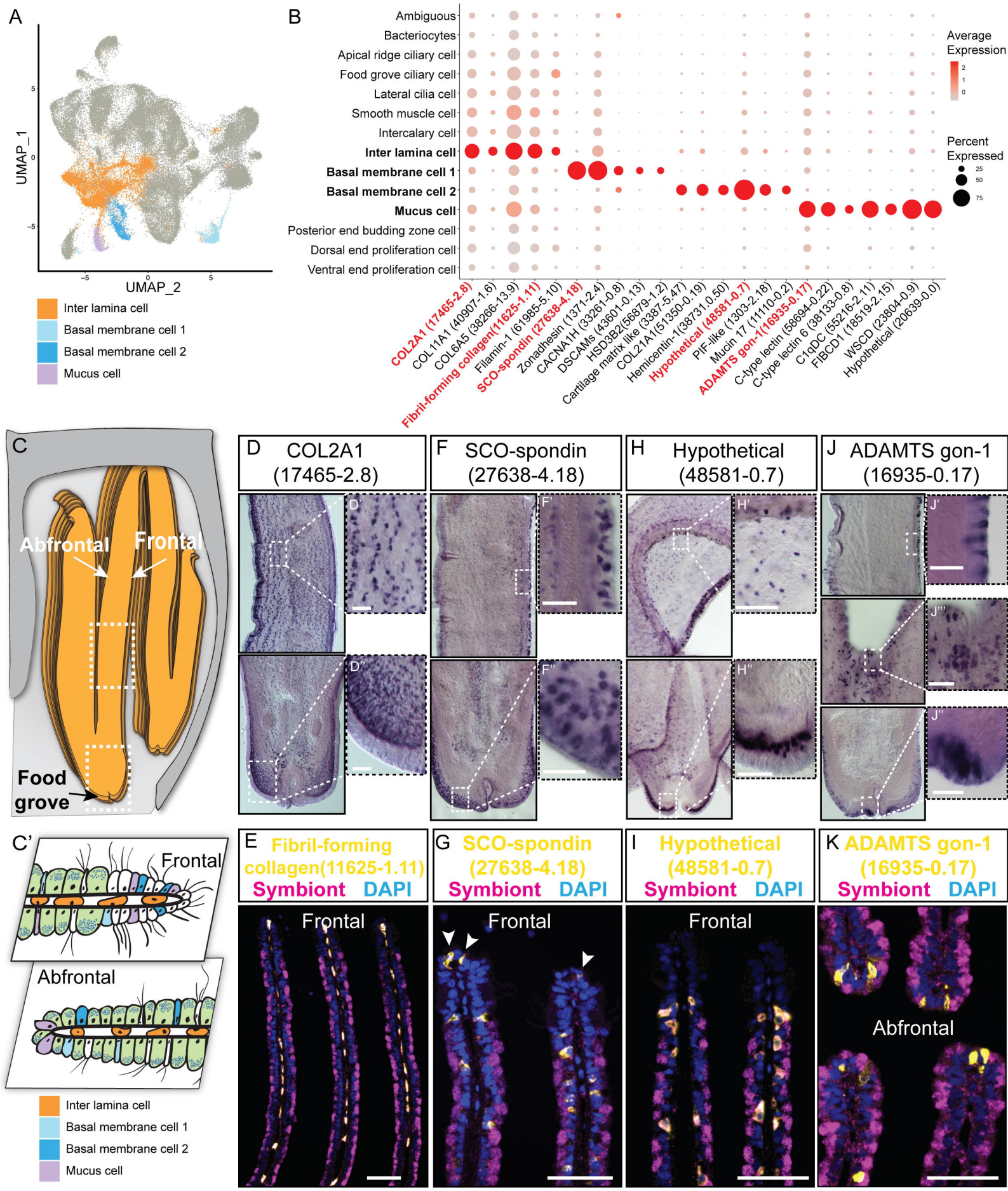
A
UMAP_1
UMAP_2
Inter lamina cell
Basal membrane cell 1
Basal membrane cell 2
Mucus cell
B
Ambiguous
Bacteriocytes
Apical ridge ciliary cell
Food grove ciliary cell
Lateral cilia cell
Smooth muscle cell
Intercalary cell
Inter lamina cell
Basal membrane cell 1
Basal membrane cell 2
Mucus cell
Posterior end budding zone cell
Dorsal end proliferation cell
Ventral end proliferation cell
Average Expression
Percent Expressed
COL2A1 (17465-2.8)
COL11A1 (40907-1.6)
COL6A5 (38266-13.9)
Fibril-forming collagen(11625-1.11)
Filamin-1 (61985-5.10)
SCO-spondin (27638-4.18)
Zonadhesin (1371-2.4)
CACNA1H (33261-0.8)
DSCAMs (43601-0.13)
HSD3B2(56879-1.2)
Cartilage matrix like (3387-5.47)
COL21A1(51350-0.19)
Hemicentin-1(38731.0.50)
Hypothetical (48581-0.7)
PIF-like (1303-2.18)
Mucin 17 (11110-0.2)
ADAMTS gon-1(16935-0.17)
C-type lectin (58694-0.22)
C-type lectin 6 (38133-0.8)
C1qDC (55216-2.11)
FIBCD1 (18519-2.15)
WSCD (23804-0.9)
Hypothetical (20639-0.0)
C
Abfrontal
Frontal
Food grove
D COL2A1 (17465-2.8)
F SCO-spondin (27638-4.18)
H Hypothetical (48581-0.7)
J ADAMTS gon-1 (16935-0.17)
C'
Frontal
Abfrontal
Inter lamina cell
Basal membrane cell 1
Basal membrane cell 2
Mucus cell
E Fibril-forming collagen(11625-1.11)
G SCO-spondin (27638-4.18)
I Hypothetical (48581-0.7)
K ADAMTS gon-1 (16935-0.17)
Symbiont DAPI
Frontal
Abfrontal

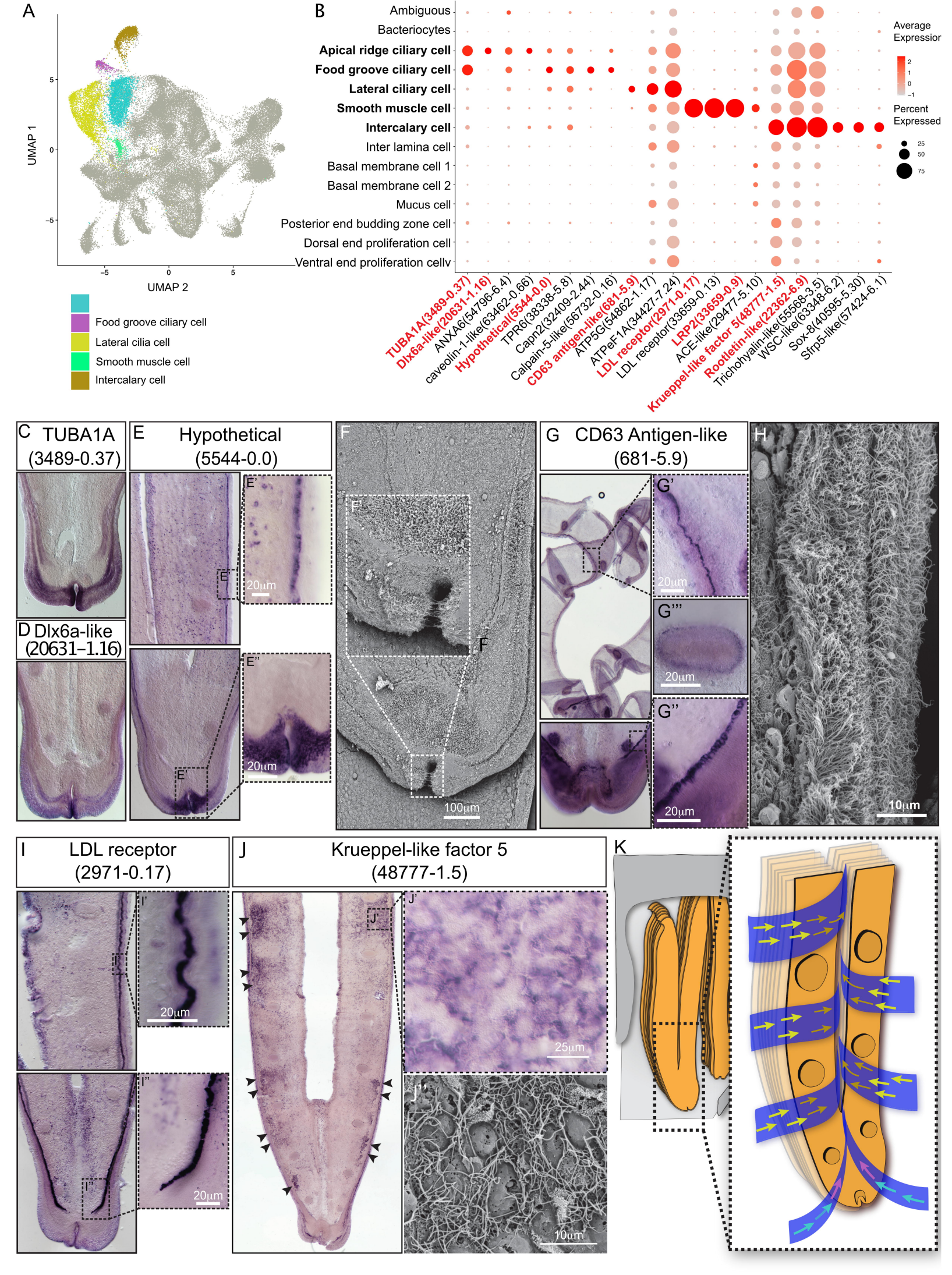
A
UMAP 1
UMAP 2
Food groove ciliary cell
Lateral cilia cell
Smooth muscle cell
Intercalary cell
B
Ambiguous
Bacteriocytes
Apical ridge ciliary cell
Food groove ciliary cell
Lateral ciliary cell
Smooth muscle cell
Intercalary cell
Inter lamina cell
Basal membrane cell 1
Basal membrane cell 2
Mucus cell
Posterior end budding zone cell
Dorsal end proliferation cell
Ventral end proliferation cellv
TUBA1A(3489-0.37)
Dlx6a-like(20631-1.16)
ANXA6(54796-6.4)
caveolin-1-like(63462-0.66)
Hypothetical(5544-0.0)
TPR6(38338-5.8)
Capn2(32409-2.44)
Calpain-5-like(56732-0.16)
CD63 antigen-like(681-5.9)
ATP5G(54862-1.17)
ATPeF1A(34427-7.24)
LDL receptor(2971-0.17)
LDL receptor(33659-0.13)
LRP2(33659-0.9)
ACE-like(29477-5.10)
Krueppel-like factor 5(48777-1.5)
Rootletin-like(22362-6.9)
Trichohyalin-like(55568-3.5)
WSC-like(63348-6.2)
Sox-8(40595-5.30)
Sfrp5-like(57424-6.1)
Average Expression
Percent Expressed
C TUBA1A (3489-0.37)
D Dlx6a-like (20631–1.16)
E Hypothetical (5544-0.0)
F
G CD63 Antigen-like (681-5.9)
H
I LDL receptor (2971-0.17)
J Krueppel-like factor 5 (48777-1.5)
K
20µm
100µm
10µm
25µm

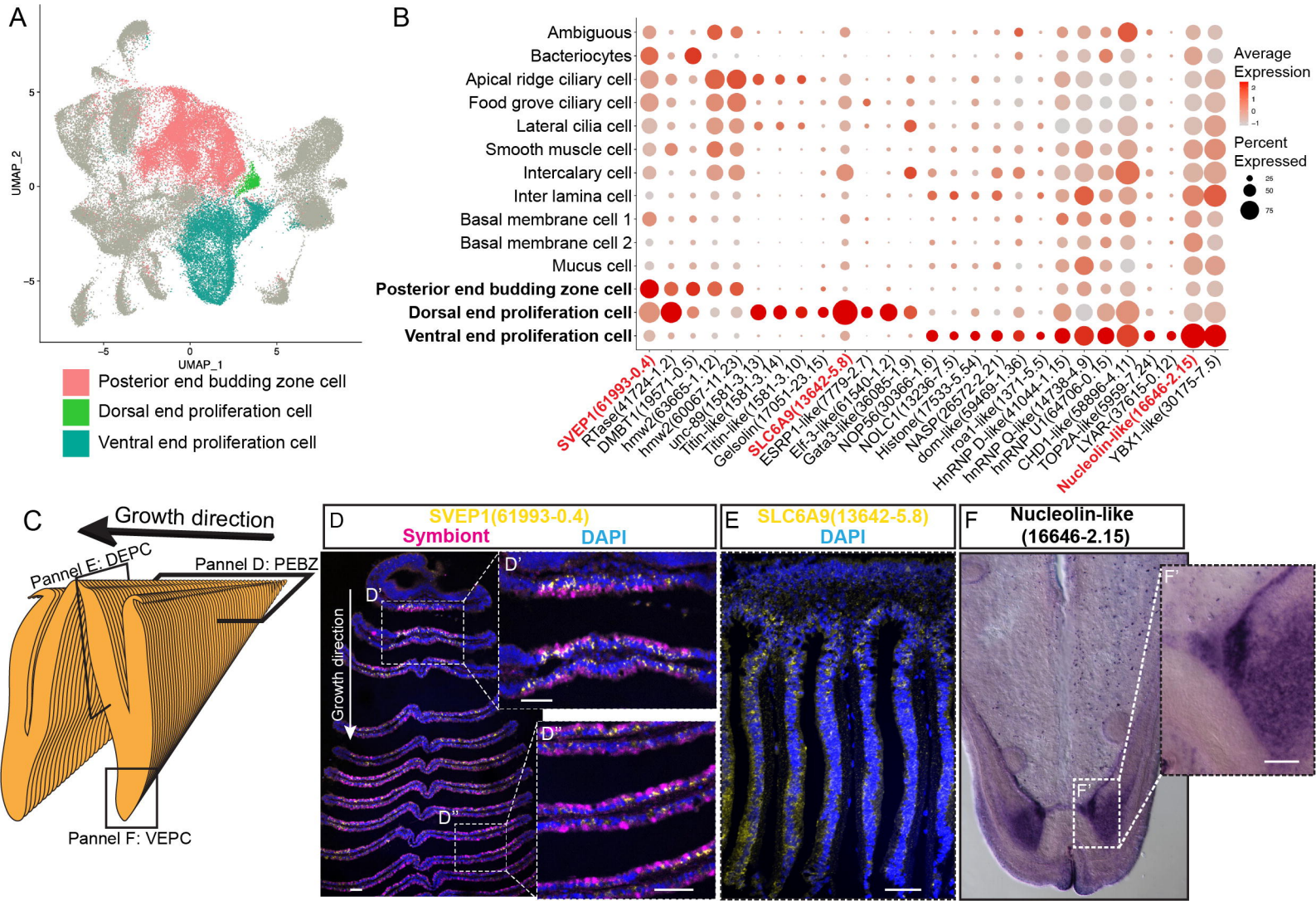
A
UMAP_2
UMAP_1
Posterior end budding zone cell
Dorsal end proliferation cell
Ventral end proliferation cell
B
Ambiguous
Bacteriocytes
Apical ridge ciliary cell
Food grove ciliary cell
Lateral cilia cell
Smooth muscle cell
Intercalary cell
Inter lamina cell
Basal membrane cell 1
Basal membrane cell 2
Mucus cell
Posterior end budding zone cell
Dorsal end proliferation cell
Ventral end proliferation cell
SVEP1(61993-0.4)
RTase(41724-1.2)
DMBT1(19571-0.5)
hmw2(63665-1.12)
hmw2(60067-11.23)
unc-89(1581-3.13)
Titin-like(1581-3.14)
Titin-like(1581-3.10)
Gelsolin(17051-23.15)
SLC6A9(13642-5.8)
ESRP1-like(7779-2.7)
Elf-3-like(61540-1.2)
Gata3-like(36085-1.9)
NOP56(30366-1.6)
NOLC1(13236-7.5)
Histone(17533-5.54)
NASP(26572-2.21)
dom-like(59469-1.36)
roa1-like(1371-5.5)
HnRNP D-like(41044-1.15)
hnRNP Q-like(14738-4.9)
hnRNP U1(64706-0.15)
CHD1-like(58896-4.11)
TOP2A-like(5959-7.24)
Nucleolin-like(16646-2.15)
LYAR-(37615-0.12)
YBX1-like(30175-7.5)
Average Expression
Percent Expressed
C
Growth direction
Pannel E: DEPC
Pannel D: PEBZ
Pannel F: VEPC
D
SVEP1(61993-0.4)
Symbiont
DAPI
Growth direction
D'
D''
E
SLC6A9(13642-5.8)
DAPI
F
Nucleolin-like
(16646-2.15)
F'

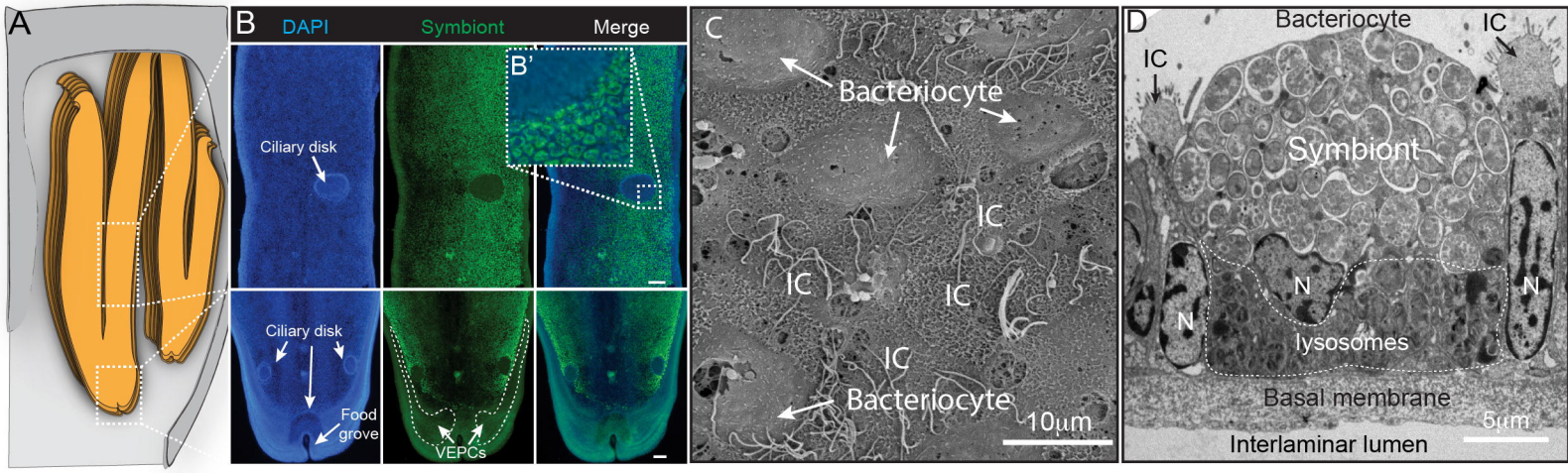
A
B
DAPI
Symbiont
Merge
B'
Ciliary disk
Ciliary disk
Food grove
VEPCs
C
Bacteriocyte
IC
IC
IC
IC
Bacteriocyte
10μm
D
Bacteriocyte
IC
IC
Symbiont
N
N
N
lysosomes
Basal membrane
Interlaminar lumen
5μm

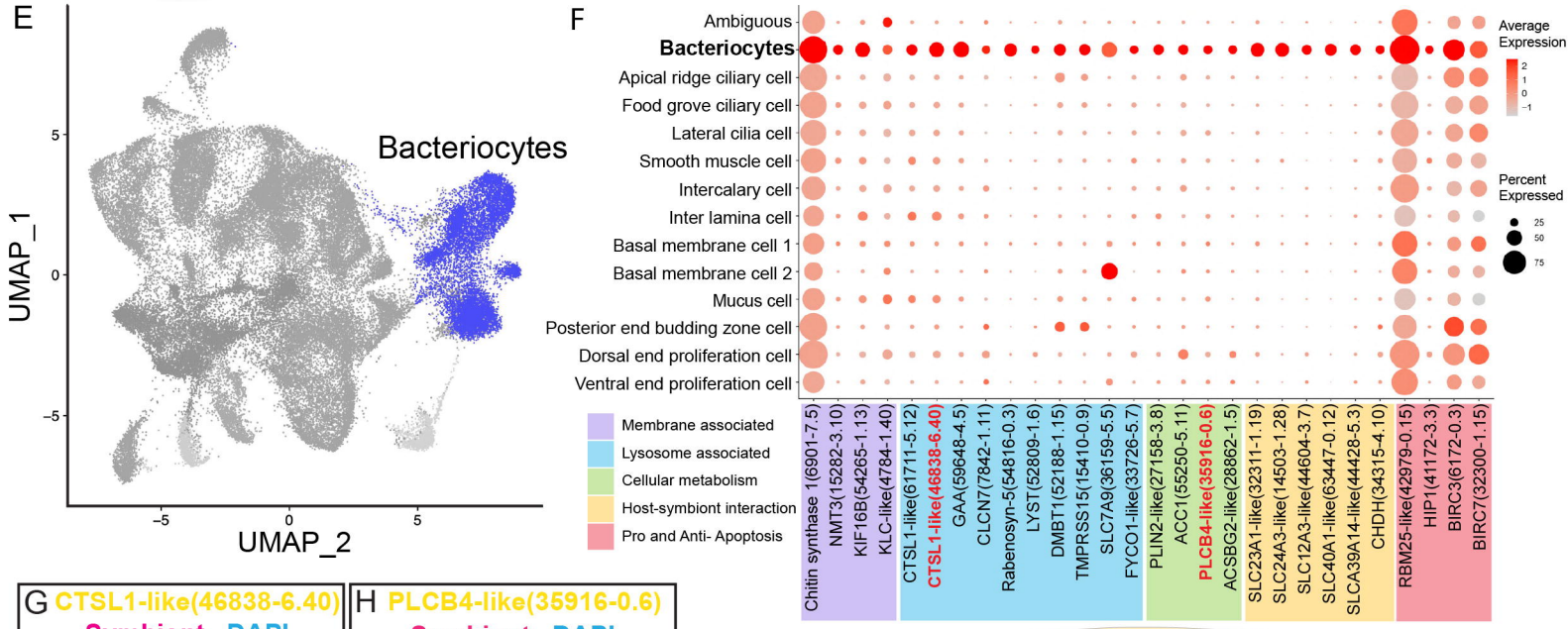
E
Bacteriocytes
UMAP_1
UMAP_2
5
0
−5
−5
0
5
F
Ambiguous
Bacteriocytes
Apical ridge ciliary cell
Food grove ciliary cell
Lateral cilia cell
Smooth muscle cell
Intercalary cell
Inter lamina cell
Basal membrane cell 1
Basal membrane cell 2
Mucus cell
Posterior end budding zone cell
Dorsal end proliferation cell
Ventral end proliferation cell
Average Expression
Percent Expressed
Membrane associated
Lysosome associated
Cellular metabolism
Host-symbiont interaction
Pro and Anti- Apoptosis
Chitin synthase 1(6901-7.5)
NMT3(15282-3.10)
KIF16B(54265-1.13)
KLC-like(4784-1.40)
CTSL1-like(61711-5.12)
CTSL1-like(46838-6.40)
GAA(59648-4.5)
CLCN7(7842-1.11)
Rabenosyn-5(54816-0.3)
LYST(52809-1.6)
DMBT1(52188-1.15)
TMPRSS15(15410-0.9)
SLC7A9(36159-5.5)
FYCO1-like(33726-5.7)
PLIN2-like(27158-3.8)
ACC1(55250-5.11)
PLCB4-like(35916-0.6)
ACSBG2-like(28862-1.5)
SLC23A1-like(32311-1.19)
SLC24A3-like(14503-1.28)
SLC12A3-like(44604-3.7)
SLC40A1-like(63447-3.12)
SLCA39A14-like(44428-5.3)
CHDH(34315-4.10)
RBM25-like(42979-0.15)
HIP1(41172-3.3)
BIRC3(6172-0.3)
BIRC7(32300-1.15)

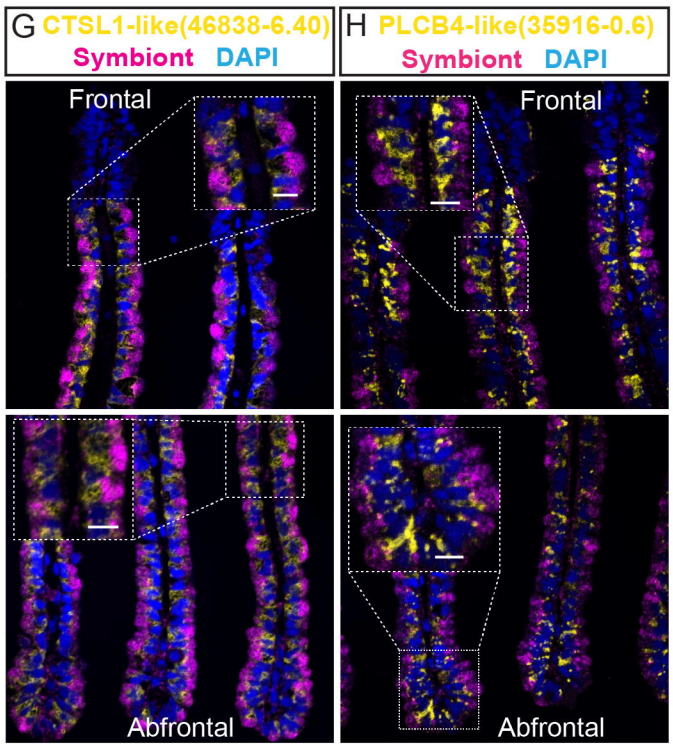
G CTSL1-like(46838-6.40)
Symbiont DAPI
H PLCB4-like(35916-0.6)
Symbiont DAPI
Frontal
Frontal
Abfrontal
Abfrontal

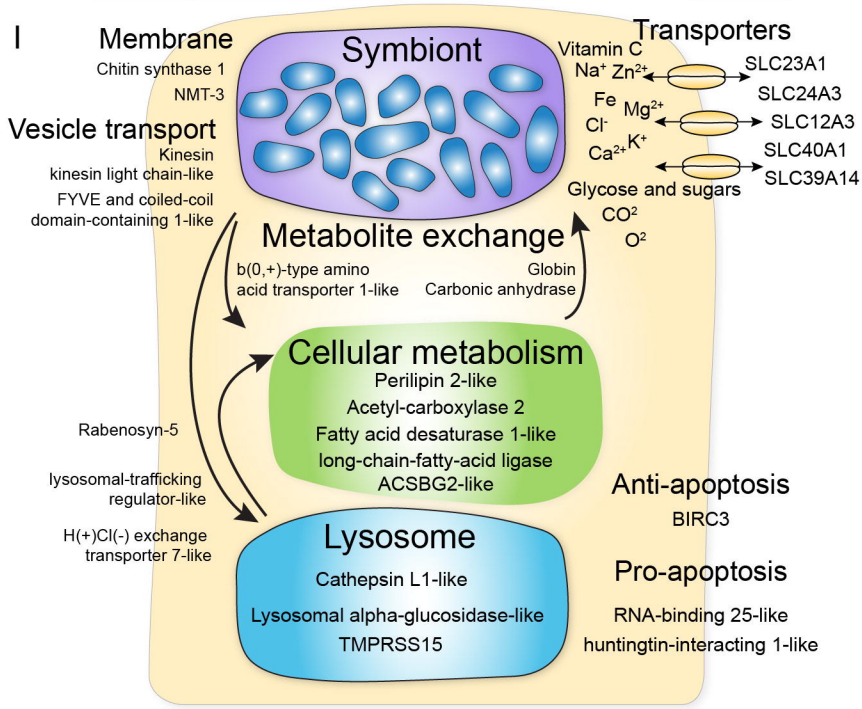
I
Membrane
Chitin synthase 1
NMT-3
Vesicle transport
Kinesin
kinesin light chain-like
FYVE and coiled-coil domain-containing 1-like
Symbiont
Transporters
Vitamin C
Na+ Zn2+
SLC23A1
SLC24A3
Fe Mg2+
Cl-
SLC12A3
Ca2+ K+
SLC40A1
SLC39A14
Glycose and sugars
CO2
O2
Metabolite exchange
b(0,+)-type amino acid transporter 1-like
Globin
Carbonic anhydrase
Cellular metabolism
Perilipin 2-like
Acetyl-carboxylase 2
Fatty acid desaturase 1-like
long-chain-fatty-acid ligase ACSBG2-like
Rabenosyn-5
lysosomal-trafficking regulator-like
H(+)Cl(-) exchange transporter 7-like
Lysosome
Cathepsin L1-like
Lysosomal alpha-glucosidase-like
TMPRSS15
Anti-apoptosis
BIRC3
Pro-apoptosis
RNA-binding 25-like
huntingtin-interacting 1-like

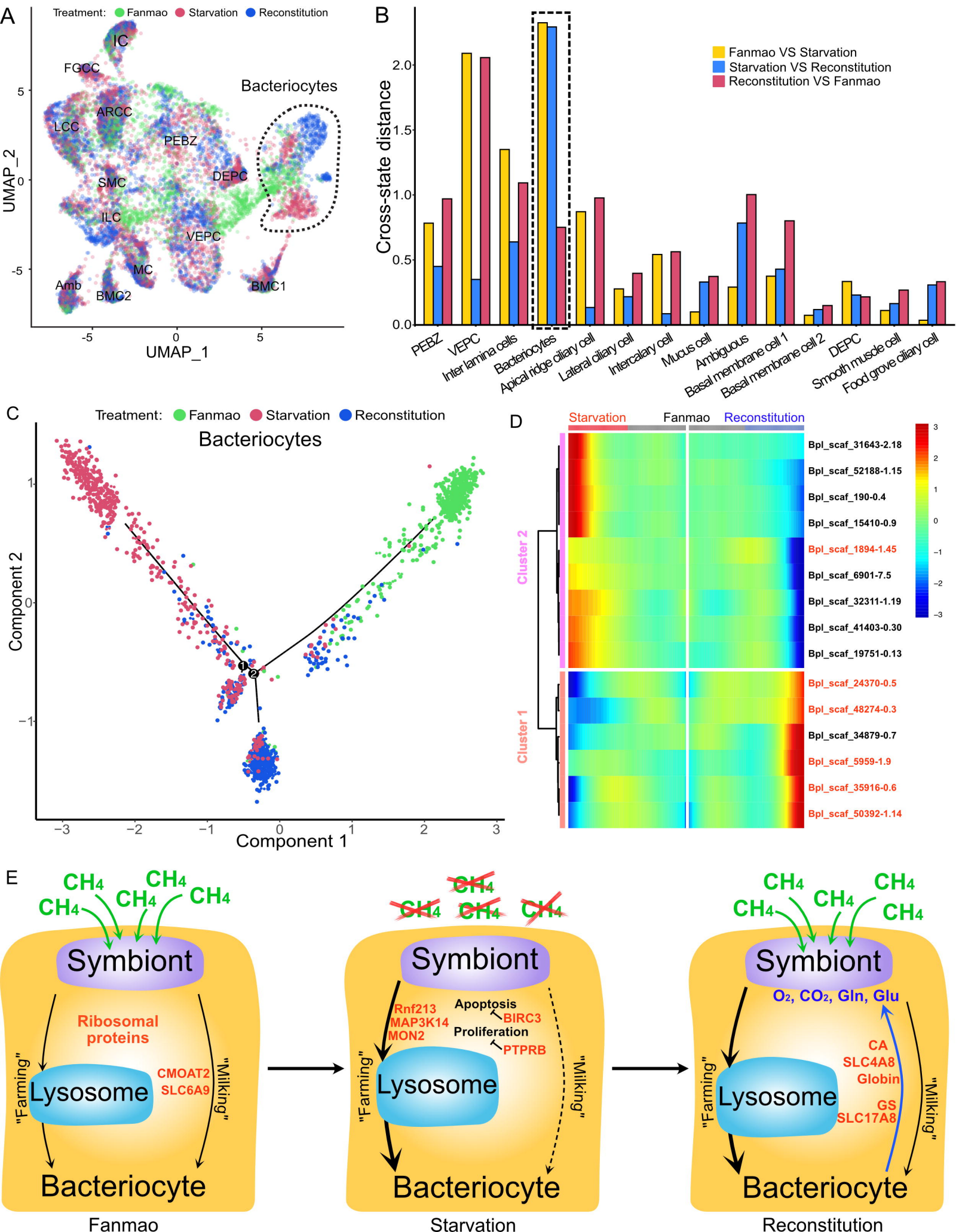
A
Treatment: Fanmao Starvation Reconstitution
IC
FGCC
Bacteriocytes
ARCC
LCC
PEBZ
SMC
DEPC
ILC
VEPC
MC
Amb
BMC2
BMC1
UMAP_2
UMAP_1
B
Fanmao VS Starvation
Starvation VS Reconstitution
Reconstitution VS Fanmao
Cross-state distance
PEBZ
VEPC
Inter lamina cells
Bacteriocytes
Apical ridge ciliary cell
Lateral ciliary cell
Intercalary cell
Mucus cell
Ambiguous
Basal membrane cell 1
Basal membrane cell 2
DEPC
Smooth muscle cell
Food grove ciliary cell
C
Treatment: Fanmao Starvation Reconstitution
Bacteriocytes
Component 2
Component 1
D
Starvation
Fanmao
Reconstitution
Cluster 2
Cluster 1
Bpl_scaf_31643-2.18
Bpl_scaf_52188-1.15
Bpl_scaf_190-0.4
Bpl_scaf_15410-0.9
Bpl_scaf_1894-1.45
Bpl_scaf_6901-7.5
Bpl_scaf_32311-1.19
Bpl_scaf_41403-0.30
Bpl_scaf_19751-0.13
Bpl_scaf_24370-0.5
Bpl_scaf_48274-0.3
Bpl_scaf_34879-0.7
Bpl_scaf_5959-1.9
Bpl_scaf_35916-0.6
Bpl_scaf_50392-1.14
E
CH4
Symbiont
Ribosomal proteins
Lysosome
CMOAT2
SLC6A9
"Farming"
"Milking"
Bacteriocyte
Fanmao
Rnf213
MAP3K14
MON2
Apoptosis
BIRC3
Proliferation
PTPRB
Starvation
O2, CO2, Gln, Glu
CA
SLC4A8
Globin
GS
SLC17A8
Reconstitution